Integrated Master in Chemical Engineering

Solubility measurements for supercritical CO_2 in polymers for offshore applications

Master Thesis

Susana Raquel Melo de Almeida

Supervisor: **Nicolas von Solms**

July 2012

Universidade do Porto
Faculdade de Engenharia
FEUP

Solubility measurements for supercritical CO_2 in polymers for offshore applications

Susana Raquel Melo de Almeida

Master Thesis

July 2012

July 2012

Acknowledgements

I would like to thank my supervisor Nicolas von Solms, for his guidance through the lasts five months. He challenged me to go further in the project and to break barriers that I supposed insuperable. I would also like to thank Zacarias Tecler for introducing me to the experimental set-up and for being positive when I was not.

I gratefully acknowledge Rasmus Lundsgaard for providing assistance with modeling, giving me the script that allows all the data modeling.

I would like to thank NKT-flexibles for the financial support which made possible the realization of this project.

Thanks to all my friends that walked with me in this journey, especially to António Campos for believing more in me than myself!

And last, but not least, I would like to thank to family for giving me the possibility to live this experience and for supporting me along all this years of my life (Muito Obrigada e Adoro-vos!)

Abstract

In order to transport supercritical carbon dioxide safely in polymer pipelines, it is necessary to understand several thermodynamic and transport properties of the polymer/gas system. With this in mind, measurements were carried out with supercritical CO_2. The most important properties are solubility and permeability in polymers. To measure the solubility a Magnetic Suspension Balance was used (Rubotherm Präzisionsmeßtechnik GmbH, Germany) and for permeability was used a 2-D permeation cell (manufactured by the Department of Chemical and Biochemical Engineering at Technical University of Denmark). Several measurements were performed with two different polymers, PVDF and XLPE.

Solubility was measured at pressures ranging from 0 to 150 bar, for PVDF, and from 0 to 300 bar, for XLPE. In both cases the measurements were performed at 45 ºC and at 90 ºC. After the data analysis, doing the needed buoyancy corrections, results are presented in grams of gas per grams of polymer. The results are also modeled with the PC-SAFT equation of state for polymers.

Permeability was measured at 45, 60, 75 and 90 °C for XLPE and at 45 °C to PVDF. In both polymers the pressure in high pressure chamber were performed at 100 bar.

The results were also analyzed to study the influence of the temperature in solubility and in permeability.

Keywords: Solubility, Diffusion, Permeability, Transport phenomena, Polymers, Carbon Dioxide, simplified PC-SAFT

Declaration

Declares, under oath, that this work is original and that all not original contributions were properly referenced with identification of the source.

July 10, 2012

_____

(Susana Raquel Melo de Almeida)

Contents

Contents i
List of Figures iv
List of Tables vi
List of Symbols vii
1 Introduction 1
2 State of the art 2
3 Theory 5
3.1 Supercritical Carbon Dioxide Properties 5
3.2 Transport Phenomena 7
3.2.1 Diffusion Coefficient 7
3.2.2 Solubility coefficient 10
3.2.3 Permeability 10
3.3 Sorption modes 12
3.3.1 Henry's Law Sorption 12
3.3.2 Langmuir-Mode Sorption 12
3.3.3 Dual-Mode Sorption 13
3.3.4 Flory-Huggins Mode 13
3.3.5 BET Mode 14
3.4 Glassy and Rubbery Polymers and Glass Transition Temperature 15
3.5 Free Volume Theory 16
3.6 Parameters Affecting Transport Characteristics 18
3.6.1 Influence of Temperature 18
3.6.2 Influence of Pressure 19
3.6.3 Influence of Crystallinity and Crosslinking 20
3.7 Polymer Samples 22
3.7.1 PVDF 22
3.7.2 XLPE 22

3.8 Methods to measure the solubility of CO_2 in polymers 23
3.8.1 Phase separation method 23
3.8.2 Pressure decay method 23
3.8.3 Gravimetric method 23
3.8.4 Chromatographic method 24
3.9 Solubility Modeling 25
4 Solubility Experiments and Modelling 27
4.1 Experimental Work 27
4.1.1 Equipment 27
4.1.2 Buoyancy 28
4.1.3 Performed tests 29
4.1.4 Experimental Procedure 29
4.1.5 Calculation method 30
4.2 Experimental Results and Discussion 33
4.2.1 PVDF 34
4.2.2 XLPE 34
4.3 Modeling 35
4.3.1 PVDF 35
4.3.2 XLPE 36
4.4 Influence of Temperature 37
5 Permeability Experiments 39
5.1 Experimental work 39
5.1.1 Equipment 39
5.1.2 Experiments Performed 40
5.1.3 Experimental procedure 40
5.1.4 Calculation method 41
5.2 Experimental Results and Discussion 42
5.2.1 PVDF 42
5.2.2 XLPE 43

5.3 Influence of Temperature 46
5.3.1 XLPE 46
6 Conclusions 47
7 List of References 48
Appendix 1 – sPC-SAFT Equations 51
Appendix 3 – Calculation Example for solubility 53
Appendix 4 – Influence of Temperature Graphs in Solubility 57
- PVDF 57
- XLPE 59
Appendix 5 – Influence of Temperature Graphs in Permeability 61
- XLPE 61

List of Figures

Figure 2.1 - Structure of a typical flexible pipe (Rubin & Wang, 2012)..... 3
Figure 3.1 - P-T phase diagram of Carbon Dioxide..... 5
Figure 3.2 - Density as a function of pressure for Carbon Dioxide (data are from NIST chemistry webbook, 2012)..... 6
Figure 3.3 - Five stages of transport phenomena for gases in polymers (Klopffer & Flaconnèche, 2001)..... 7
Figure 3.4 - Calculation of time-lag (Flaconnèche, et al., 2001)..... 9
Figure 3.5 - Classic sorption modes of the penetrant in the polymer matrix. (Klopffer & Flaconnèche, 2001)..... 12
Figure 3.6 - Structure of a semi-crystalline polymer [37]..... 20
Figure 3.7 - Squematic representation of a Crosslinking structure (Callister, 2007)..... 21
Figure 4.1 - Different positions of MSB..... 27
Figure 4.2 – Picture of the open MSB..... 28
Figure 4.3 - Buoyancy effect: (a) in vacuum; (b) in a pressurized system..... 29
Figure 4.4 - Corrected weight as a function of corrected density..... 31
Figure 4.5 - Solubility of the penetrant as a function of Density to XLPE at 90°C up to 200 bar..... 32
Figure 4.6 - Experimental results for solubility of Carbon Dioxide in PVDF at 45 °C and 90 °C. The dots represent the measurements at 45 °C and the lines with dots represent the measurements at 85 °C..... 34
Figure 4.7 - Experimental results for solubility of Carbon Dioxide in XLPE at 45 °C and 90 °C. The dots represent the measurements at 45 °C and the lines with dots represent the measurements at 90 °C..... 34
Figure 4.8 - sPC-SAFT solubility correlations for CO_2 in PVDF at 45 °C and 85 °C The binary parameter is selected to reproduce the lower pressure data. The dots are the average of experimental results..... 35
Figure 4.9 - sPC-SAFT solubility correlations for CO_2 in PVDF at 45 °C and 85 °C. The binary parameter is selected to reproduce the intermediate pressure data.. The dots are the average of experimental results..... 35
Figure 4.10 - sPC-SAFT solubility correlations for CO_2 in PVDF at 45 °C and 85 °C The binary parameter is selected to reproduce the highest pressure data.. The dots are the average of experimental results..... 35

Figure 4.11 - sPC-SAFT correlations for solubility of CO_2 in XLPE at 45 °C and 90 °C. The binary parameter is chosen so that the model reproduces the low pressure data. The dots are the average of experimental results.....36
Figure 4.12 - sPC-SAFT correlations for solubility of CO_2 in XLPE at 45 °C and 90 °C. The binary parameter is chosen so that the model reproduces the intermediate pressure data. The dots are the average of experimental results. 36
Figure 4.13 - sPC-SAFT correlations for solubility of CO_2 in XLPE at 45 °C and 90 °C,. The binary parameter is chosen so that the model reproduces the high pressure data.. The dots are the average of experimental results.....36
Figure 5.1 – Permeation Cell assembled prior to a run 39
Figure 5.2 - Schematic set-up of high-pressure 2-D permeation cell.....40
Figure 5.3 - Pressure in High Pressure and in Low Pressure Chamber for PVDF at 45 °C.....42
Figure 5.4 – Detail of measurement with PVDF at 45 °C with high pressure chamber at 100 bar.....42
Figure 5.5 - Pressure in High Pressure and in Low Pressure Chamber for XLPE at 45 °C. 43
Figure 5.6 - Pressure in High Pressure and in Low Pressure Chamber for XLPE at 60 °C. 43
Figure 5.7 - Pressure in High Pressure and in Low Pressure Chamber for XLPE at 75 °C. 44
Figure 5.8 - Pressure in High Pressure and in Low Pressure Chamber for XLPE at 90 °C. 44
Figure A2.1 - Measurement with Argon to obtain the real weigh and volume of the sample..54
Figure A2.2 - Solubility of the penetrant as function of Density to XLPE at 90 °C up to 200 bar 55
Figure A2.3 - Experimental results for Absolute solubility of Carbon Dioxide in XLPE at 90 °C 56
Figure A3.1 - Arrhenius plot for experimental solubility of CO_2 at three pressures, in PVDF..57
Figure A3.2 - Arrhenius plot for the modeled values of solubility (fitted to lower pressure data), for three pressures, in PVDF.....57
Figure A3.3 - Arrhenius plot for the modeled values of solubility (fitted to intermediate pressure data), for three pressures, in PVDF.....58
Figure A3.4 - Arrhenius plot for the modeled values of solubility (fitted to high pressure data), for three pressures, in PVDF.....58
Figure A3.5 - Arrhenius plot for experimental solubility at three pressures, in XLPE. 59
Figure A3.6 - Arrhenius plot for solubility modeled, respecting the lower pressure, at three pressures, in XLPE.....59
Figure A3.7 - Arrhenius plot for solubility modeled, respecting the intermediate pressure, at three pressures, in XLPE. 60
Figure A3.8 - Arrhenius plot for solubility modeled, respecting the upper pressure, at three pressures, in XLPE.....60

Figure A4.1 - Plot of 1/T vs ln(Pe) for the PVDF/CO_2 system at $P_{High\ Pressure\ Chamber}$ = 100 bar ..61

List of Tables

Table 4.1 - Tests performed for CO_2 solubility in polymers.....29
Table 4.2 - Solubility for each Pressure, Temperature and Polymer (average values).....33
Table 4.3 - The pre-exponential term in the Arrhenius equation for solubility. The results are for the solubility measured from the experimental work and modeled to reproduce the lower, intermediate and upper pressures. 37
Table 4.4 - Heat of dissolution of a penetrant mole in the matrix in the Arrhenius equation for solubility. The results are for the measured solubility modeled solubility for the lower, intermediate and upper pressures. Literature values are also presented. 37
Table 4.5 - Results of the pre-exponential term in the Arrhenius equation for solubility. The results are for the solubility from the experimental work and modeled respecting the lower, intermediate and upper pressures. 38
Table 4.6 - Results of the heat of dissolution of a penetrant mole in the matrix in the Arrhenius equation for solubility. The results are for the solubility from the experimental work and modeled respecting the lower, intermediate and upper pressures. 38
Table 5.1 - Conditions for the permeability experiments.....40
Table 5.2 - Results of Permeability and Diffusion through PVDF at $P_{High\ Pressure\ Chamber}$ = 100 bar and 45 °C.....42
Table 5.3 - Results for Permeability through XLPE at $P_{High\ Pressure\ Chamber}$ = 100 bar to 45, 60, 75 and 90 °C 45

List of Symbols

Abbreviations

STP	Standard Temperature and Pressure
XLPE	Cross-link Polyethylene
PVDF	Polyvinylidene Fluoride
MSB	Magnetic Suspension Balance
PC-SAFT	Perturbed chain statistical associating fluid theory
EOS	Equations of state

Theory

A	Membrane area	cm^2
a	Thermodynamic activity of the component in the mixture	
A_d	Parameter which depends on the penetrant size and shape	
b	"hole affinity" constant	
B_d	Parameter of the available free volume fraction	
C	Concentration	$g \cdot l^{-1}$
C_D	Concentration of molecules dissolved in the polymer by an ordinary dissolution process	$g \cdot l^{-1}$
C_H	Concentration of trapped molecules by adsorption on specific sites	$g \cdot l^{-1}$
C'_H	"hole saturation" constant	
D	Diffusion Coefficient	$cm^2 \cdot s^{-1}$
D_T	Diffusivity related with mobility – free volume theory	$cm^2 \cdot s^{-1}$
D_0	Pre-exponential term of Arrhenius equation for diffusion	
D^*	Diffusivity coefficient in a completely amorphous polymer	$cm^2 \cdot s^{-1}$
E_D	Apparent activation energy of the diffusion process	$kJ \cdot mol^{-1}$
E_P	Apparent activation energy of the permeation process	$kJ \cdot mol^{-1}$
f	Free volume fraction	

f_u	Fugacity	Pa
J	Flux of the penetrant through a membrane	g· cm^{-2}·s^{-1}
k	Constant	
k_D	Proportionality constant of Henry's law	
l	Thickness of the membrane	cm
m_d	Mobility of diffusion molecules	
M_t	Mass uptake of the gas at time t	g
M_∞	Mass uptake of the gas at long time (equilibrium)	g
n	Type of transport mechanism	
p	Pressure	bar
p^0	Saturation vapour pressure	bar
p_1^0	Liquid-vapour equilibrium pressure	bar
Pe	Permeability Coefficient	cm^3_{STP}·cm^{-1}·bar^{-1}·s^{-1}
Pe_0	Pre-exponential term of Arrhenius equation for permeability	
Q	Amount of gas	g
R	Ideal gas constant	J·K^{-1}·mol^{-1}
S	Solubility Coefficient	g_{gas}·$g_{polymer}^{-1}$
S_0	Pre-exponential term of van't Hoff equation for solubility	
S^*	Solubility coefficient in a completely amorphous polymer	g_{gas}·$g_{polymer}^{-1}$
T	Absolute temperature	K
t	Time	s
T_g	Glass transition temperature	K
V	Volume	cm^3
V_1	Partial molar volume of the penetrant	kJ·mol^{-1}
∇C	Concentration gradient between both sides of the membrane	g·l^{-1}
ΔH_{cond}	Molar heat of condensation	kJ·mol^{-1}
ΔH_l	Partial molar heat of mixing	kJ·mol^{-1}

ΔH_s	Enthalpy of sorption	kJ·mol^{-1}
ΔP	Mean pressure difference	bar

Greek Letters

θ	Time-lag	s
ρ	Density	mol·l^{-1}
ϕ_1	Volume fractional of the permeant in the polymer	
ϕ_2	Volume fractional of the polymer in the mixture	
χ	Enthalpic interaction parameter	
χ_l	Flory-Huggins interaction parameter	
α	Thermal expansion coefficient of the free volume	
β	Compressibility	
γ	Coefficient of concentration	
δ	Square roots of the cohesive energy densities	
ϕ_a	Volume fractional of the amorphous phase	
β_{chain}	Chain immobilization factor	
τ	Tortuosity factor	

Underscripts

cell	permeation cell at downstream side
end	after time t
f	free
occ	occupied
start	at time zero
Tot	total

Solubility Experiments and Modeling

H	Holding Force	N
F_G	Gravitational force	N
g	Acceleration due the gravity	$m \cdot s^{-2}$
m	Mass	g
V	Volume	cm^3
p	Pressure	bar
B	Buoyancy	N
$corr.Weight$	Weight given by MSB	g
$corr.Density$	Corrected value for density	$g \cdot cm^{-3}$
S	Solubility	$g_{gas} \cdot g_{polymer}^{-1}$
S_{abs}	Absolute solubility	$g_{gas} \cdot g_{polymer}^{-1}$
k_{ij}	Binary interaction parameter	

Underscripts

SC+S	sample container/ sample system
SC	sample container
S	sample
ads	adsorbed gas
Bal	weight read in the balance

Greek Letters

ρ	density	$g \cdot cm^{-3}$

Appendix 1

A	Helmholtz energy	J
$\tilde{a}$	Reduced Helmholtz energy	
d	Temperature-dependent segment diameter	nm
g	Radial distribution function	
k	Boltzmann's constant	$J \cdot K^{-1}$
m	Segment number	
N	Number of molecules	
T	Temperature	K
x	Mole fraction	

Greek Letters

ε	Depth of the dispersion potential	J
η	Volume fraction	
ρ	Total number density	nm^{-3}
σ	Segment diameter	nm

Superscripts

assoc	association
disp	dispersion
hc	hard chain
hs	hard sphere
id	ideal

1 Introduction

The purpose of this project is to understand how temperature and pressure influence solubility and permeability of carbon dioxide, in supercritical state, in polymers. The goal of understanding these properties is the safety transportation of carbon dioxide in pipelines, for offshore application. The transport of carbon dioxide is required for many applications, for example, in the field of gas and oil industry.

The pipeline has a polymeric inner liner and two possible candidates for that inner are PVDF and XLPE, both produced by NKT-flexibles. The function of the inner is preventing the escape of the gases, preventing damage to the other layers in the structure of pipeline. The carbon dioxide will be transported at high temperature and pressure, this means that is necessary to reach these conditions in the laboratory and use equipments prepared to work with supercritical state. The used equipments were a Magnetic Suspension Balance, for measuring the solubility, and a 2-D permeation cell for measure the permeability.

Thesis outline

Chapter 1 - provides introduction to the project, the importance and objectives;

Chapter 2 - gives the succinct presentation of the problem, the context and the application;

Chapter 3 - in this chapter is presented the theoretical context of the transport of carbon dioxide. This section provides a summary of the relevant fundamentals from literature, some models that have been proposed and developed. It will show that the transport phenomena depends strongly on the polymer structure, temperature and pressure. In this chapter is also presented a brief introduction to modeling with sPC-SAFT.

Chapter 4 - all details of the experimental work to understand the solubility, the results, the discussion of the results and some graphs with the most suitable model for each temperature. The direct effect of influence of temperature in solubility is also presented, with parameters of Arrhenius Equation.

Chapter 5 - the details of experimental work to understand the permeability are presented. The direct application of the theory leads to results of permeability for the desired temperatures and pressure.

Chapter 6 and 7 - conclusion and references are provided

2 State of the art

Along the years supercritical fluids have been used in several applications, especially as solvents or antisolvents or in the polymer processing: e.g. polymer modifications, polymer composites, polymer blending, microcellular foaming and in polymer synthesis. Supercritical carbon dioxide is also used in these applications; is a good solvent for polar and low molecular weight components, but in general it is a very poor solvent for high weight polymers. (Nalawade et al., 2006)

Carbon dioxide has two distinct applications in the field of gas and oil industry, the first one is in the production from ultra-deep water high pressure reservoirs with high CO_2 contents, and the second one in reinjection of CO_2. The reinjection can be driven by a wish to reduce CO_2 emissions as in Carbon Capture and Storage (CCS) projects, but also as a method for Enhanced Oil Recovery (EOR). In all cases it is likely that CO_2 will be present in supercritical state.

For the last 35 years flexible pipes have been a key component in offshore oil and gas production. This kind of pipes presents advantages when compared with rigid pipes such as the faster installation time and the better adaptation to the changes in field layout. These advantages make the flexible pipes a more economical solution.

The flexible pipes are constructed from concentric layers of polymeric and steel materials. In order to preserve the flexibility of the pipe construction the layers are not bound together. In Figure 2.1 is possible see the structure of the main layers in a flexible pipe.

The flexible pipes have been used offshore as a reliable solution for high pressure methane. However this component has a lower solvent power than carbon dioxide and this will influence on the performance of polymers in contact with it. In addiction carbon dioxide is soluble in water causing the reduction of pH value. The combination of aqueous environments with reduced pH promotes hydrolysis of some polymers, and the same environment can corrode metals.

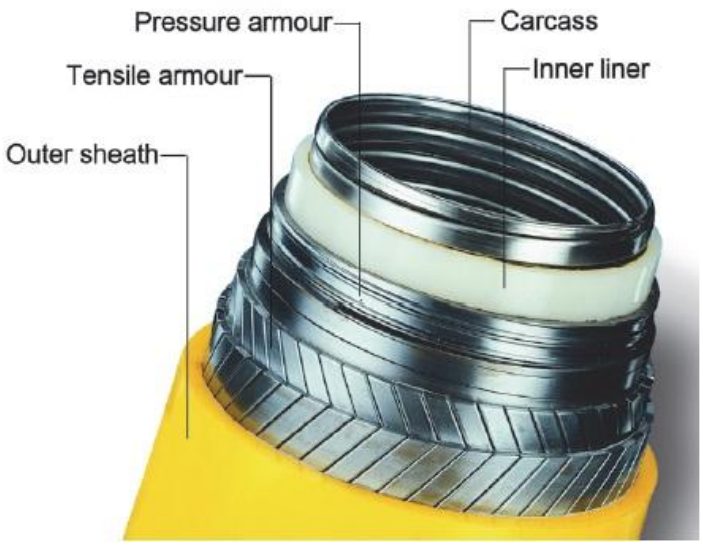

Figure 2.1 - Structure of a typical flexible pipe (Rubin & Wang, 2012)

The potential impacts in pipeline structure that are necessary take into account are related with three areas:

- **Impact on polymeric materials in contact with high pressure CO_2**

The high solvent power of carbon dioxide can result in swelling and increased solubility of gases in the polymers and loss of plasticizer in plasticized polymers. The swelling, the uptake and the loss of plasticizer leads to changes of mechanical properties of the polymer which changes the performance of the polymer and consequently the potentiality of the pipe. The swelling can also result in the increasing of the permeation of the gas through the polymer. The increases of solubility of the gas in the polymer may lead to increased risk of blistering damage from rapid decompression.

- **Flexible pipe annulus environment in high pressure CO_2 applications**
- **Corrosion of metallic materials in contact with CO_2**

The used materials in the inner liner are HDPE, PA11, PA12, XLPE and PVDF. PA11 and PA12 are plasticized polymers, so the loss of plasticizer will be very likely and some problems can occur when this polymer is exposed to high pressure CO_2. The swelling and the hydrolysis can also be problematic to these materials. HDPE has a relative low allowable operational temperature. So this polymer has not been considered as suitable materials for inner liners for high pressure and temperature CO_2.

XLPE is a cross-linked poly ethylene manufactured by NKT-Flexibles; this polymer has a high degree of cross-linking and unique material properties and is expected to be resistant to swelling when exposed to high pressure carbon dioxide. Moreover, XLPE is not plasticized, so the loss of plasticizer will not be an issue.

PVDF is a single layer non-plasticized layer; the single layer design ensures that gas is not trapped between liner layers which can lead to the collapse of the inner in gas applications. The XLPE and PVDF are the most suitable candidates for inner liner materials for applications with carbon dioxide at high pressure and temperature (Rubin & Wang, 2012).

3 Theory

3.1 Supercritical Carbon Dioxide Properties

A supercritical fluid is a fluid which has a temperature and pressure above its critical values, i.e. in the critical region, shown in Figure 3.1. The density of fluids near the critical point is very sensitive to small changes of pressure. Figure 3.2 is a plot of the density as a function of pressure for carbon dioxide. Fluids in this state possess characteristics of both gases and liquids. For example they can permeate through solids (as a gas), but can also dissolve certain substances, for example a liquid. Supercritical carbon dioxide is a clean and a versatile solvent and is a promising alternative to organic solvents such as chlorofluorocarbons. It is non-toxic, non-flammable, chemically inert and inexpensive.

The supercritical stage of carbon dioxide is readily attained: the conditions are T_c = 30.9782 °C and P_c = 73.773 bar and can be removed from the system by simple depressurization. (Nalawade et al., 2006)

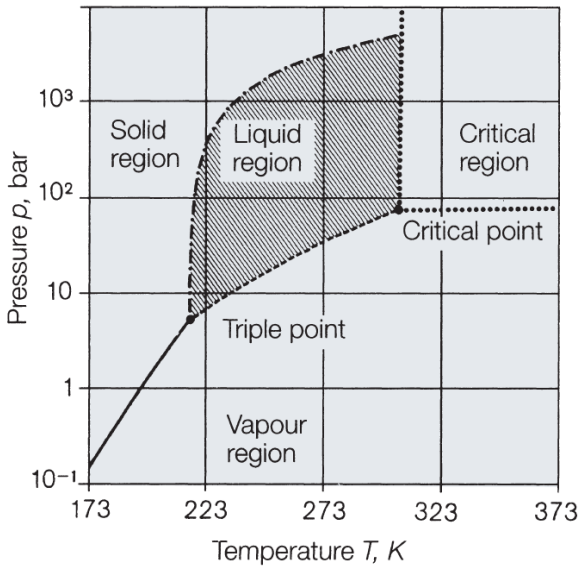

Figure 3.1 - P-T phase diagram of Carbon Dioxide (Union Engineering)

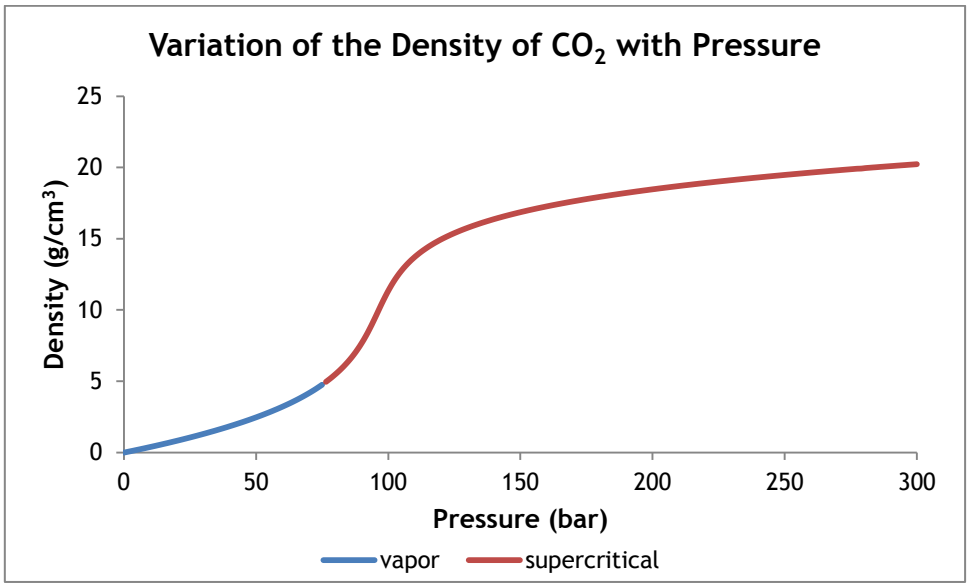

Figure 3.2 - Density as a function of pressure for Carbon Dioxide (data are from NIST chemistry webbook, 2012)

Many polymers have a high degree of swelling and plasticize at high pressures in the presence of carbon dioxide. The solubility of carbon dioxide in many polymers is substantial; this depends on pressure and temperature, but also on weak interactions with the chain group in the polymer. Carbon dioxide absorved in the polymer causes a considerable reduction in the viscosity of molten polymers due to an increase of free volume. Several other physical properties of polymers are altered such as the density, diffusivity and the swollen volume.

3.2 Transport Phenomena

The transport of gases through a polymer membrane is related to the properties of the material that is crossed by the gas molecules.

The phenomena of gas transport through a polymer can be decomposed into 5 steps, as presented in Figure 3.3. The steps are as follows:

- Diffusion through the limit layer on the side corresponding to the higher partial pressure (upstream side);
- Adsorption of the gas (by chemical affinity or by solubility) by the polymer;
- Diffusion of the gas inside the membrane polymer;
- Desorption of the gas at the side of lower partial pressure;
- Diffusion through the limit layer of the downstream side. (Klopffer & Flaconnèche, 2001)

The transport phenomena can be grouped into three transport coefficients: diffusion, solubility, and permeability.

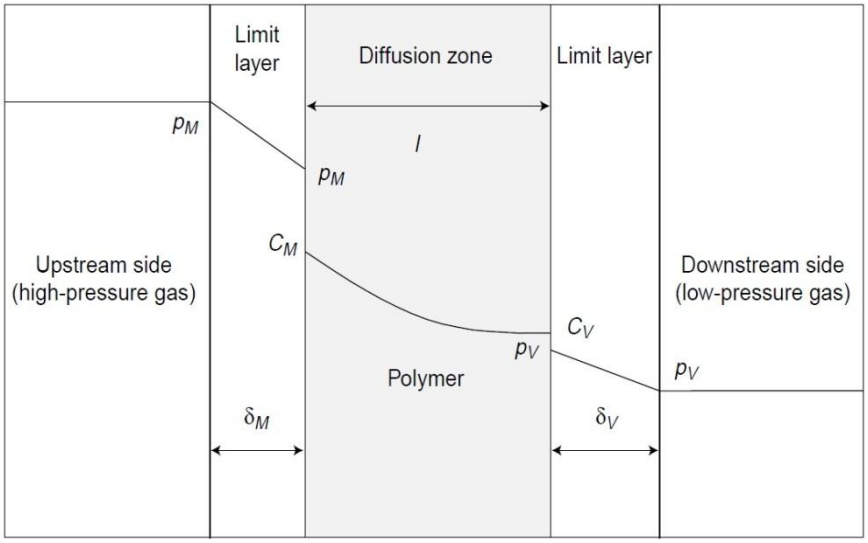

Figure 3.3 - Five stages of transport phenomena for gases in polymers (Klopffer & Flaconnèche, 2001)

3.2.1 Diffusion Coefficient

Diffusion is the passage of small molecules from one place to another due to random molecular motion. The amount of gas, Q, that crosses the membrane area, A, during the time, t, is called the flux, J. (Flaconnèche et. al., 2001)

$$J = \frac{Q}{At} \tag{3.1}$$

Fick's first law establishes a relation between the flux of gas diffusing through a membrane and the concentration gradient between both sides of the membrane:

$$J = -D\nabla C \tag{3.2}$$

where D is the diffusion coefficient (cm^2/s). For the case of unidirectional diffusion the amount of gas per unit of membrane volume is equal to the increase of the gas concentration with respect to time. It is possible to write:

$$-\frac{dJ}{dx} = \frac{dC}{dt} \tag{3.3}$$

Combining equation (3.2) and (3.3) and assuming that D is constant in the membrane leads to Fick's second law:

$$\frac{dC}{dt} = -D\frac{d^2C}{dx^2} \tag{3.4}$$

When the polymer, with thickness l, is exposed to a gas and the diffusion coefficient is constant, the integration of equation (3.7) results in:

$$J\int_0^l dx = -D\int_{C_1}^{C_2} dC \tag{3.5}$$

Then:

$$J = \frac{D(C_1 - C_2)}{l} \tag{3.6}$$

where C_1 and C_2 are the gas concentration in the membrane on the high pressure side and on the low pressure side, respectively and l is the thickness of the membrane. It is sometimes possible to obtain the value of D by the time-lag method developed by Barrer (1939). When t tends towards very long times steady state is reached and a straight line is observed. Before the system reaches steady state the flux and the concentration vary with time in every point inside the membrane and from the interception of the time axis with the extrapolated linear steady state it is possible to obtain the time-lag. This time can be thought of as the time until pseudo steady state is reached.

If D is independent of the concentration, the diffusion coefficient is related to the time-lag by the following simple equation:

$$D = \frac{l^2}{6\theta} \tag{3.7}$$

Where θ is the time-lag.

This relation demonstrates that establishing the steady-state concentration profile within the membrane takes longer for small D.

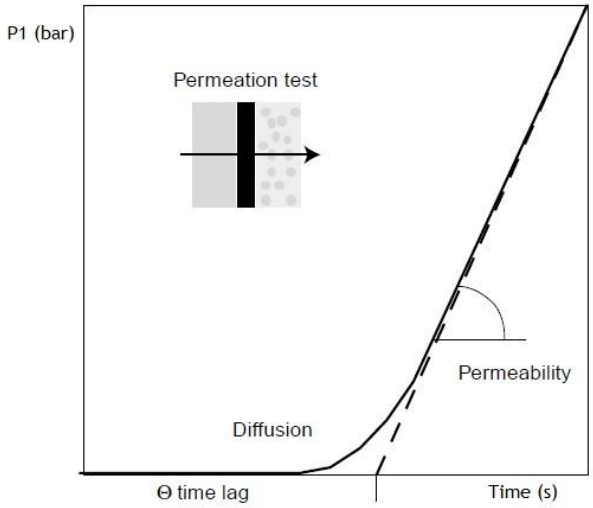

Figure 3.4 - Calculation of time-lag (Flaconnèche, et al., 2001)

Mechanisms of diffusion

The polymer structure is an important parameter to take into account when considering the transport of gases through a polymer, since the transport in a glassy polymer is quite different from transport in a rubbery polymer. It is possible to classify diffusion in terms of three categories which depend on the relative mobilities of the gas and the polymer:

- Fickian – the rate of diffusion is smaller than the relaxation modes of the polymeric matrix. The adsorption equilibrium is quickly reached with this type of diffusion, the boundary conditions are independent of the time and do not depend on swelling kinetics.
- Non-Fickian – the diffusion is faster when compared with the simultaneous relaxation processes of the polymer. This mechanism has a strong dependence on the swelling kinetics.
- Anomalous diffusion – this refers to a process where the diffusion and the polymer relaxation rates are comparable. The sorption and the transport of molecules are affected by the presence of pre-existing microvoids in the matrix; the penetration is mainly dependent on the structure of the polymer.

3.2.2 Solubility coefficient

Henry's law relates the concentration of a gas in the polymer with pressure:

$$C = k_D p \tag{3.8}$$

Where p is the pressure and k_D is the proportionality constant of Henry's law. The Henry's law constant represents the solubility coefficient when there is no concentration dependence. That means:

$$C = S \cdot p \tag{3.9}$$

Combining the equation (3.6) and (3.9) it is possible to re-write the next equation:

$$J = \frac{DS\left(p_1 - p_2\right)}{l} \tag{3.10}$$

The solubility coefficient, S, is a thermodynamic parameter and depends on the polymer-penetrant interactions as well as on gas condensability. This coefficient is a function of temperature, pressure and concentration. The solubility coefficient is expressed in $g_{gas}/g_{polymer}$.

3.2.3 Permeability

The product DS is called the permeability coefficient.

$$Pe = DS \tag{3.11}$$

The coefficient of permeability is the product of a kinetic factor, D, which reflects the dynamics of the penetrant-polymer system and of a thermodynamic term, S, which depends on the penetrant-polymer interactions. So the permeability coefficient represents the ease with which the penetrant crosses the polymer membrane under a pressure gradient.

Combining the equation (3.1) and the equation (3.10) it is possible to write the following equation, which is used to determine the value of the permeability coefficient.

$$Pe = \frac{l}{A} \cdot \frac{\rho_{end} - \rho_{start}}{\rho_{STP}} \cdot \frac{V_{cell}}{\Delta P \cdot t} \tag{3.12}$$

where l is the membrane thickness, A is the membrane polymer area, ρ_{end} and ρ_{start} are the gas density to temperature and pressure after time t and at time zero (given by webbook.nist.gov/), ρ_{STP} is the gas density at Standard Temperature and Pressure, V_{cell} is the volume of permeation cell at downstream side, ΔP is the mean pressure difference between downstream pressure and upstream pressure and t is the total time of measurement.

Pe depends on the nature of the polymer, the gas, the upstream and downstream pressure and the temperature, and is typically expressed in $cm^3_{STP}/(cm \cdot bar \cdot s)$.

3.3 Adsorption modes

The adsorption is a term used to describe the capacity of the gas to penetrant in the polymer matrix. It is possible to have more than one type of adsorption in the same polymer membrane. The thermodynamics of the penetrant-polymer system, in particular the nature and the force of the interactions, determine the amount of penetrant in the polymer matrix at equilibrium and the adsorption mode.

The five classic cases of adsorption are presented in Figure 3.5.

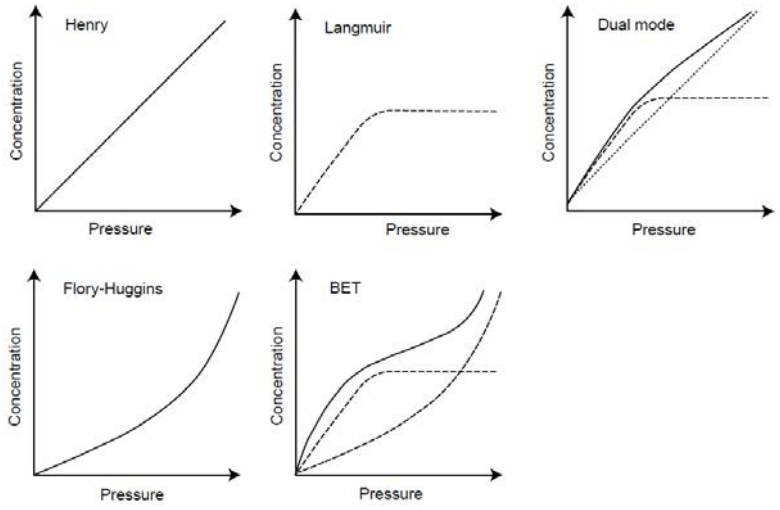

Figure 3.5 - Classic adsorption modes of the penetrant in the polymer matrix. (Klopffer & Flaconnèche, 2001)

3.3.1 Henry's Law Sorption

This is the simplest case of sorption: the gas is considered ideal and there is a linear relation between the penetrant concentration and its partial pressure, as shown by equation (3.8)

This sorption is only observed at low pressure when the penetrant-polymer interactions and penetrant-penetrant interactions are weaker than polymer-polymer interactions, so the gas is randomly dispersed in the matrix. (Klopffer & Flaconnèche, 2001)

3.3.2 Langmuir-Mode Sorption

In this type of sorption the predominant interaction is penetrant-polymer. The molecules of the penetrant occupy specific sites in the polymer (pre-existing microvoids or high-area inorganic fillers). When all the sites are occupied, only a small amount of penetrant can solubilize subsequently. The penetrant concentration is given by an equation of the form

$$C_H = \frac{C'_H bp}{1+bp} \tag{3.13}$$

Where C'_H is the Langmuir capacity factor or "hole saturation" constant and b the Langmuir site affinity parameter.

3.3.3 Dual-Mode Sorption

This model was proposed to describe curves in the case of sorption of low-activity gases in glassy polymers. It considers the existence of two populations of diffusing molecules: molecules dissolved in the polymer by an ordinary dissolution process with a concentration C_D, and molecules trapped by adsorption on the specific sites (microvoids or holes) with a concentration C_H. If it is supposed that at equilibrium pressure, p, the concentration of the adsorped molecules in the polymer by an ordinary mechanism dissolution, C_D, obeys Henry's law (equation (3.8)), and that the concentration of molecules sorbed in a limited number of pre-existing microcavities is given by the Langmuir equation (3.13), it is possible to write the following equation:

$$C = C_D + C_H = k_D p + \frac{C'_H bp}{1+bp} \tag{3.14}$$

This model is based on the assumption that gases do not interact with the polymer matrix (there is no swelling).

3.3.4 Flory-Huggins Mode

This sorption mode assumes that the penetrant-polymer interactions are weak compared with penetrant-penetrant interactions and the solubility coefficient increases continuously with increasing pressure. Two physical interpretations of this behavior are possible; the plasticization of the polymer by the sorbed molecules or the association of clusters in the case of water-hydrophobic polymer systems. The solubility can be calculated as follows:

$$\ln a = \ln \frac{p}{p^0} = \ln \phi_1 + (1-\phi_1) + \chi (1-\phi_1)^2 \tag{3.15}$$

where a is the thermodynamic activity of the component in the mixture (vapor pressure of the gas (p) divided by the saturation vapor pressure (p^0) at the experimental temperature), ϕ_1 is the volume fraction of the permeant in the polymer and χ the enthalpic interaction parameter between the polymer and the solute.

3.3.5 BET Mode

The BET mode combines the Langmuir and Flory-Huggins modes and is representative of the adsorption of water in highly hydrophilic polymers. Initially the water molecules are strongly sorbed in specific sites, corresponding to polar groups, then, at higher pressure, a clustering process may occur.

3.4 Glassy and Rubbery Polymers and Glass Transition Temperature

The temperature at which the polymer passes from the glassy state to a rubbery state is called the glass transition temperature, T_g. At this temperature the molecules that were virtually frozen in position below T_g begin to experience rotational and translational movements above T_g. Some amorphous polymers are cross-linked, as is the case for XLPE; this has the effect of increasing the glass transition temperature as the cross-linking restricts the molecular movements (Callister, 2007).

Transport mechanisms are different in rubbery and glassy polymers (temperature above or below the glass transition temperature).

Glassy polymers

Below the glass transition temperature the polymer is in a glassy state. In this state the transport mechanisms are not completely understood. Chain mobility is restricted, the only movements seen are vibration and the polymers are easily broken. In glassy polymers the penetration of the gas is low, but the size selectivity is very good.

If the polymer is in a glassy state the three coefficients, Pe, D and S, may not be precisely determined. A polymer in the glassy state has a specific volume, bigger than the specific volume of equilibrium. This difference, due to the non-equilibrium character of the glassy state, is at the origin of the non-linearity of the sorption isotherm. The plasticization effect is when a polymer is exposed to a vapour and the gas molecules change the polymer structure; this causes a decrease in T_g and an increase in specific volume. (Klopffer & Flaconnèche, 2001)

Rubbery polymers

Above the glass transition temperature the polymer is in a rubbery state. Rubbery polymers are flexible and respond rapidly to external stress. The penetrance of the gas is much faster in this stage, but the size selectivity is lower.

3.5 Free Volume Theory

The basic idea of this theory is that a diffusing molecule can only move from one position to another when, in its neighborhood, the local free volume exceeds a certain critical value, this means a sufficient empty space. In the case of amorphous polymers, the coefficients S and D can be related to the free volume. The free volume is given by the following equation:

$$f = \frac{V_f}{V_{Tot}} = \frac{V_{Tot} - V_{occ}}{V_{Tot}} \tag{3.16}$$

Where V_{Tot} is the total volume (the sum of the occupied volume, V_{occ}, and the free volume, V_f)

The mobility of a penetrant depends on the probability of it finding a hole of sufficient size that allows its displacement. This mobility can be related to the diffusivity as follows:

$$D_T = RT \cdot A_d \exp\left(\frac{-B_d}{f}\right) = RT \cdot m_d \tag{3.17}$$

Here m_d is the mobility of the diffusing molecules relative to the polymer, A_d is a parameter which depends on the penetrant size and shape, B_d is a characteristic parameter of the available free volume fraction and f is the fractional free volume that is given by:

$$f = \phi_1 f_1 + \phi_2 f_2 \tag{3.18}$$

Where ϕ is the volume fraction and f the free volume fraction of the component i.

The solubility coefficient is only a function of penetrant-polymer interactions, but experimentally a change in the solubility with f has been observed. The solubility coefficient can be written in terms of the interaction parameter and fractional free volume:

$$S = \frac{f}{f_1 p_1^0 \exp(1 + \chi_1)} \tag{3.19}$$

Where χ_1 is the Flory-Huggins interaction parameter and p_1^0 is the liquid-vapour equilibrium pressure of the gas at temperature T (saturated vapour pressure).

The free volume fraction depends on three thermodynamics variables: the temperature, T; the hydrostatic pressure, p applied to the system (penetrant pressure); and the penetrant concentration, which can be expressed as a volume fraction:

$$f(T,p,C) = f_{ref}(T_{ref}, p_{ref}, 0) + \alpha(T - T_{ref}) - \beta(p - p_{ref}) + \gamma C \quad (3.20)$$

The first term of this equation represents the fractional free volume of the system in a reference state, this means the pure polymer at T_{ref} and p_{ref}. The second term characterises the increase of f due to thermal dilation, where α is the thermal expansion coefficient of the free volume. The third term shows how the free volume decreases during the hydrostatic compression, where β is the compressibility ($\beta = \chi_l - \chi_g$, the coefficients χ are the compressibility of the liquid and glassy states). The last term is a measure of the penetrant effectiveness in increasing the free volume, γ is a coefficient of concentration (Klopffer & Flaconnèche, 2001; Andreasen et. al, 2008)

3.6 Parameters Affecting Transport Characteristics

3.6.1 Influence of Temperature

The solubility coefficient is represented by van't Hoff equation:

$$S = S_0 \exp\left(-\frac{\Delta H_S}{RT}\right) \tag{3.21}$$

The diffusion and permeability coefficients are well represented by Arrhenius equations:

$$D = D_0 \exp\left(-\frac{E_D}{RT}\right) \tag{3.22}$$

$$Pe = Pe_0 \exp\left(-\frac{E_P}{RT}\right) \tag{3.23}$$

where T is the absolute temperature, R the universal gas constant, ΔH_S is the enthalpy of sorption, E_D is the apparent activation energy of the diffusion process and E_P is the apparent activation energy for the permeation process. The pre-exponential terms represent the limiting values of the various transport coefficients for so-called infinite molecular agitation ($T \to \infty$) (Klopffer & Flaconnèche, 2001)

The energy for the permeation process is equal to the sum of the enthalpy of sorption and the energy for the diffusion process.

$$E_P = E_D + \Delta H_S \tag{3.24}$$

The enthalpy of sorption can be expressed as:

$$\Delta H_S = \Delta H_{cond} + \Delta H_1 \tag{3.25}$$

Where ΔH_{cond} is the molar heat of condensation, this term is always negative and small for gases, and ΔH_1 is the partial molar heat of mixing. The partial molar heat of mixing is a small and positive term, which can be estimated from the cohesive energy densities of the penetrant and the polymer by using Hildebrand's theory:

$$\Delta H_1 = V_1(\delta_1 - \delta_2)^2 \phi_2^2 \tag{3.26}$$

The solubility parameters , δ_1 and δ_2, are the square roots of the cohesive energy densities of the penetrant and the polymer, V_1 is the partial molar volume of the penetrant and ϕ_2 the volume fraction of the polymer in the mixture.

In the case of CO_2, ΔH_S is negative due to the ΔH_{cond}'s strong contribution and a decrease of the solubility will be observed with increasing temperature. This is because the gas has more difficulty condensing in the polymer when the temperature is higher.

The activation energy is by definition the energy necessary for a molecule to jump from one level of energy to another one; this energy is always a positive quantity. Therefore, D increases with the increasing of temperature. This effect is the consequence of an increase in free volume, directly related to the bulk expansion of the polymer whereby the diffusion process is facilitated.

The increase of the diffusion coefficient with temperature is dominant compared with the solubility coefficient decrease, so the permeability increases with increasing temperature. (Klopffer & Flaconnèche, 2001; Costello & Koros, 1992)

3.6.2 Influence of Pressure

The effect of the permeability coefficient on pressure depends on the diffusing molecule type. Some literature (Stern et al. 1972, 1986) conclude that the pressure influence could be explained as the result of two opposite phenomena: one related to the hydrostatic pressure and the other due to the diffusing molecule concentration within the matrix, each of these effects leading to a different dependence of permeability, both effects are explain below.

Diffusion Coefficient

When the pressure on the upstream side of the membrane is increased, two opposite effects may occur:

- A hydrostatic pressure increase leading to an increase of the polymer density, by reducing the free volume inside the polymer;
- The pressure increase corresponds to an increase of the penetrant concentration in the membrane. These diffusing molecules can plasticize the macromolecular chains, which mean an increase in free volume.

The first effect tends to retard the diffusion process by reducing the segmental motions whereas the second enhances it.

Solubility Coefficient

For high pressures strong anomalies can be observed with deviations from Henry's law. In this case, it may be necessary to express the solubility terms of fugacity, f_u, and not pressure, to take in to account the gas molecules compressibility:

$$C = S(T) f_u \tag{3.27}$$

However, when the concentration of gas inside the polymer reaches higher values, this relation is no longer valid and it is necessary to use a thermodynamic model which better describes the influence of the gas concentration on the solubility, such as an equation of state model.

3.6.3 Influence of Crystallinity and Crosslinking

Crystallinity is the fraction of polymer which is crystalline; the region where the molecules are well arranged in a regular order. The region where the molecules are arranged in a random disorganized state is called the amorphous region, as can be seen in Figure 3.6

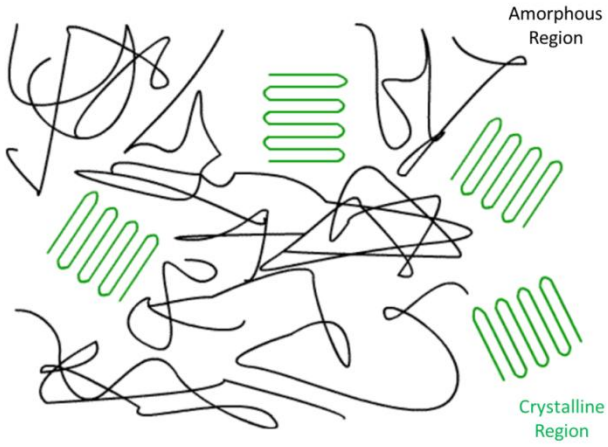

Figure 3.6 - Structure of a semi-crystalline polymer (http://www.doitpoms.ac.uk/tlplib/polymerbasics/crystallinity.php)

Sorption and diffusion take place in the amorphous regions and the crystalline regions act as excluded volumes for the sorption process and are impermeable barriers for the diffusion process. The existence of crystalline regions does not seem to influence the sorption mode in the amorphous region.

Crystalline regions have two effects on the gases diffusion. The first is the increase of effective path length of diffusion, and, the second is the apparent reduction of the polymer

chain's mobility in the amorphous phase. The crystallinity has a crosslinking effect or "anchoring" action which tends to immobilize the amorphous chains.

The solubility and diffusion coefficients can be written as a function of these new factors:

$$S = S^* \phi_a \tag{3.28}$$

$$D = \frac{D^*}{\beta_{Chain} \tau} \tag{3.29}$$

Where D^* and S^* are the diffusion and solubility coefficients in a completely amorphous polymer, ϕ_a the volume fraction of the amorphous phase, β_{Chain} is a chain immobilization factor and τ is the tortuosity factor (the more tortuous pathway that a diffusing molecule must take in a semicrystalline polymer).

Some crystalline structures allow the passage, by diffusion and sorption, of small molecules of penetrant; this can be explained by a more open structure or small density difference between the crystalline and the amorphous regions (Klopffer & Flaconnèche, 2001). Nevertheless, the rate of transport of gas in the polymers will decrease with increasing crystallinity.

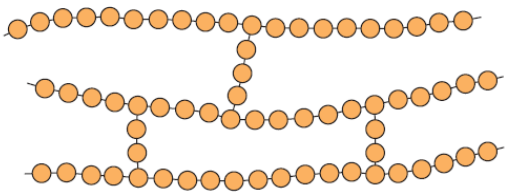

Figure 3.7 - Squematic representation of a Crosslinking structure (Callister, 2007)

When the degree of crosslinking increases, the diffusion coefficient decreases. The pre-exponential term, D_0, and the activation energy, E_D, (equation 3.22) both increase with increasing crosslinking level, but the polymer chains mobility is reduced. The combination of these effects leads to a drop in diffusion coefficient.

3.7 Polymer Samples

3.7.1 PVDF

The polyvinylidene fluoride, more known by PVDF, is a semi-crystalline polymer whose amorphous fraction is rubbery at room temperature. PVDF is a copolymer consisted in 67% poly (vinylidene fluorideco-chloro trifluoro ethylene), 33% polyvinylidene fluoride and small amounts of high-density polyethylene. The density of PVDF is 1.77 g/cm^3 and the crystalinity was estimated in 38%. PVDF is prepared to operate at temperatures up to 130 °C.

The polymer is thermally stable and possesses good resistance to corrosive chemicals and organic compounds. The most common ways to manufacture PVDF are suspension and solution. (von Solms et al., 2005)

3.7.2 XLPE

XLPE is a new method developed by NKT Flexibles to cross-link HDPE using peroxide in combination with infrared radiation. The degree of cross-linking is higher, around 90%, compared with the typical 75% for the silane-based process. This technique is used to improve the mechanical properties of HDPE. The crystallinity of XLPE is between 45 and 50% and is possible operate ate 90 °C. (Procida & Rishøj Nielsen, 2007)

3.8 Methods to measure the solubility of CO_2 in polymers

In the last decade a number of methods to measure the solubility at high pressure and temperature have been published, some of these are presented here (Nalawade et. al., 2006).

3.8.1 Phase separation method

This method is applicable to low viscosity polymers, because the mixing is relative easy. The polymer is exposed to CO_2 at the desired pressure in an autoclave; after a few hours, samples are taken from the two phases, a polymer-rich phase and CO_2-rich phase. The system should be in equilibrium. The amount of CO_2 in the polymer-rich phase determines the solubility of CO_2 in the polymer (Sameer, 2006).

3.8.2 Pressure decay method

The polymer and CO_2 are put in a closed system. The sorption of CO_2 in the polymer causes a reduction of pressure inside the system. The amount of CO_2 present initially is calculated with the pressure, temperature, the volume of the system (empty) and the volume occupied by the polymer (Sameer, 2006).

With this method it is necessary to take into account the swelling of the sample, for example from an equation of state. The pressure, temperature and swelling of the polymer are used to calculate the amount of free volume when the equilibrium is reached (when there is no change in the pressure of the system). The difference between the initial and final amounts of CO_2 gives the amount of CO_2 dissolved in the sample (Sameer, 2006).

3.8.3 Gravimetric method

In this method the weights of the polymer free of CO_2 and with sorbed CO_2 are used and the difference between the two weights is the amount (in grams) of CO_2 dissolved in the sample.

This method has some advantages over the other methods described here: smaller amounts of sample are needed, if a microbalance is used it is very sensitive to weight changes and a shorter measuring time is required.

One way to measure the weight is using a MSB (Magnetic Suspension Balance), developed by Kleinrahm and Wagner (1986). The weight difference is determined by measuring the force necessary to support the sample, inside a sample container, without having contact with the microbalance. An additional advantage is that the balance can be tared and calibrated during the measurements. However, it is still necessary to take into account the swelling of the polymer for the buoyancy correction (Sameer, 2006).

3.8.4 Chromatographic method

A very small film (micrometers) of polymer is used in this method. The polymer is the stationary phase and CO_2 the mobile phase. The measurement of the retention volume of a tracer determines the CO_2 solubility in the polymer.

The major advantage in this method is that thermodynamic equilibrium is reached very fast. A recent experimental setup was developed for measuring the swelling of the polymer in situ. This arrangement allows monitoring of the swelling of the polymer in real time. The swelling during the measurement can be used to calculate the diffusion, and the swelling in the equilibrium stage to calculate the solubility. (Sameer, 2006)

3.9 Solubility Modeling

Modern equations of state are an increasingly used tool to understand, predict and correlate the solubility of gases in polymers. At low pressure Henry's law is a useful relation that can be applied in gas-polymer systems, but above a critical gas concentration the gas sorption isotherm begins to deviate significantly. At moderate pressures this deviation can be modeled empirically by a Langmuir isotherm. It is possible, using the parameters determined at lower pressure, to extrapolate to solubility at high pressure, but this increases the inaccuracy of the data modeling. Furthermore, equations based on the Flory-Huggins lattice theory do not take into account the free volume of the polymer, which is an essential parameter in predicting the dependence of solubility on pressure, temperature and solution composition.

The commonly used EOS models for polymer/CO_2 systems are conveniently divided into three categories, depending on whether they are based on lattice theory, cubic EOSs or off-lattice theory. The discussion of these models is beyond the scope of this work.

Simplified PC-SAFT Equation

In addition to the measurement of the solubility of supercritical carbon dioxide in the polymers referred to previously, the solubility was modeled with simplified PC-SAFT (perturbed-chain statistical associating fluid theory).

PC-SAFT is an equation of state initially proposed by Gross and Sadowki (2001), who found diverse successful applications, especially in systems containing polymers and co-polymers, both at low and at high pressure.

More recently von Solms et al. (2003) developed a simplified version of PC-SAFT which is easier to apply and faster from a computational point of view, keeping, however, the precision of the original PC-SAFT. The sPC-SAFT (simplified PC-SAFT) has been applied to complex polymer-solvent systems (Neela and von Solms, 2008; von Solms et al., 2005). The relevant sPC-SAFT equations are given in Appendix 1.

However, this equation (like many others) has a limitation when applied to polymers. The necessary parameters (chain length, segment diameter and energy) to apply this equation are estimated using the vapor pressure and the liquid state density. However this is not possible for polymers, which are not volatile.

Kouskoumvekaki et al. (2004) presented a method to estimate these parameters which uses the properties of the monomers that constitute the polymers. The monomer parameters

are then extrapolated to the polymers. The objective of this project was not to obtain new parameters and those obtained by Lundsgaard (2011) for both polymers and supercritical CO_2 have been used here.

4 Solubility Experiments and Modelling

4.1 Experimental Work

4.1.1 Equipment

The Magnetic Suspension Balance (MSB) consists of a balance which enables the weighing of samples in almost all environments at controlled temperature and pressure, while the balance itself remains at ambient conditions. The sample is placed in a sample container which is connected to a permanent magnet. Under the balance there is an electromagnet that attracts the magnet whenever there is an electric current passing through it. This makes it possible to find the mass of the Sample Container/Sample system (MP_1 in Figure 4.1). The density of the gas at the current pressure and temperature conditions is determined by measurement of the mass of the sample container (with sample)/sinker system (MP_2 in figure 4.1), where the sinker weight and mass are both previously known. The buoyancy is measured and the density is obtained. Figure 4.2 shows a picture of the MSB without the heating system and with all the components identified.

The equipment is connected to a thermostat bath to keep the system temperature constant. Depending on the operating temperature, either distilled water or glycerin is used. The temperature is measured by a Pt-100 thermocouple which is installed in the system.

To keep the pressure constant an ISCO water pump is used; the pump maintains the pressure in the system using water as hydraulic fluid. The equipment is connected to a computer through the MessPro software, which records temperature, pressure, weight of the system and the density as a function of time. The software also records the .equ file, which corresponds to the value of each variable in the equilibrium state.

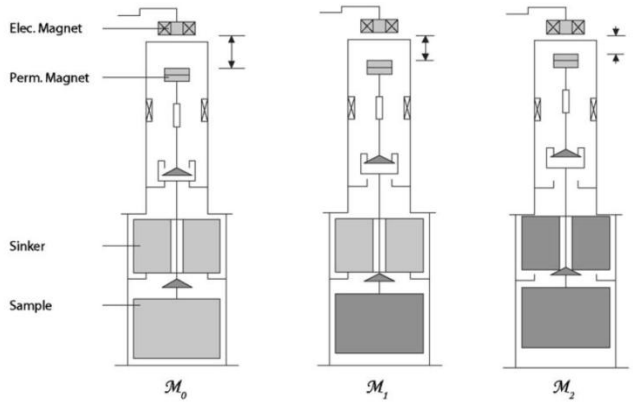

Figure 4.1 - Different positions of MSB

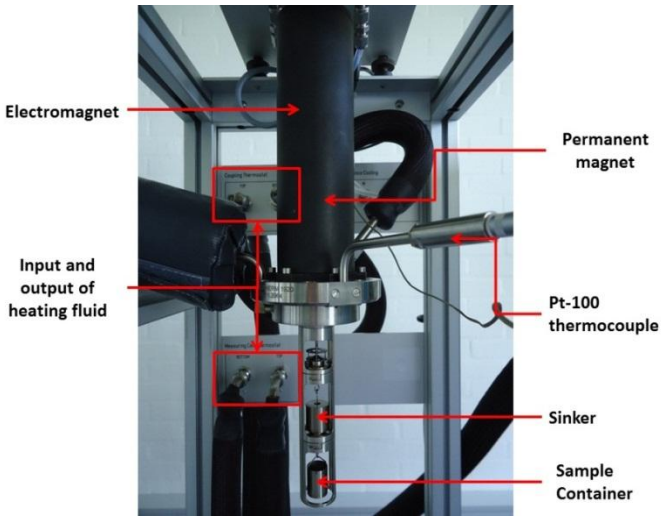

Figure 4.2 – Picture of the open MSB

4.1.2 Buoyancy

Buoyancy is an unavoidable effect experienced when performing solubility experiments using a gravimetric method, where solubility is obtained as a weight difference between a loaded and an unloaded sample. In order to obtain accurate measurements it is necessary to quantify and correct for this effect.

When under vacuum (no surrounding atmosphere) the holding force (H), which is determined by the balance, is equal to the gravitational force (F_G). In this case the mass of the sample is the same than the mass read in the display. The equilibrium of forces is shown in Figure 4.3 (a).

$$H = F_G = m \cdot g \tag{4.1}$$

Where g is the acceleration due to gravity and m the mass of the sample.

If the sample is located in a fluid at pressure P (greater than zero) and density ρ a new force appears, the buoyancy (B).

$$B = (\rho \cdot V) g \tag{4.2}$$

Where V, is the volume of the sample. The mass of the sample is then not the same as the number on the display and the correction due to buoyancy is given by the equation:

$$m = m_{Bal} + \rho \cdot V \tag{4.3}$$

Here m_{Bal} is the value read in the balance, ρ is the density of the atmosphere surrounding the sample and V is the volume of the sample. (Rubotherm - Operating Procedure (2009))

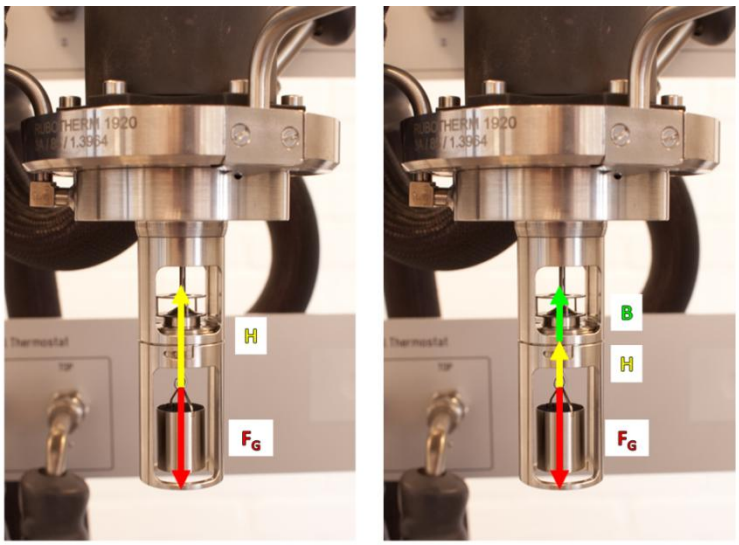

Figure 4.3 - Buoyancy effect: (a) in vacuum; (b) in a pressurized system.

4.1.3 Performed tests

Both tests were performed with the polymers PVDF and XLPE.

Solubility was measured according to the temperature and pressure conditions shown in Table 4.1.

Table 4.1 - Tests performed for CO_2 solubility in polymers

	Pressure (bar)				
Temperature (°C)	75	100	150	200	300
45	●	●□	●	□	□
90	●	●□	●	□	□

Where ● corresponds to the tests performed with the PVDF polymer, and □ to the tests performed with the XLPE polymer.

4.1.4 Experimental Procedure

The polymer is cut into small disks, approximately 8.78 mm in diameter, and placed in the sample container. The equipment is closed and the conditions desired for the measurement

(pressure, temperature, gas to be used – reference gas or measurement gas – and time of every segment) are defined in the MessPro software.

Before starting the measurement with gas, the polymer is evacuated to remove the adsorbed atmospheric gases present in the polymer. This evacuation takes at least 2 h before each measurement.

To obtain the solubility value two measurements need to be performed, firstly with an inert gas (Argon), and then with the desired gas (Carbon Dioxide). In the first measurement the real value of the mass and of the volume of the sample placed in the container are obtained (since Argon is essentially insoluble in the polymer), and in the second measurement the solubility value is obtained. The measurement with inert gas is performed in the same pressure range that is used to make the measurement with carbon dioxide, in order to have uniform data.

For each measurement a suitable number of pressure intervals was chosen, the idea being to gradually increase the pressure to the desired pressure. In the measurements performed here the pressure is increase by 20 or 40 bar from the previous pressure, depending on the final desired pressure. The time taken to achieve equilibrium can vary from hours to days.

4.1.5 Calculation method

Measurement with Argon

With the data provided by the MSB the plot shown in Figure 4.4 is obtained. The sample mass and the volume of the container/sample system can then obtained using the ordinate at the origin and the slope of the tendency line, respectively.

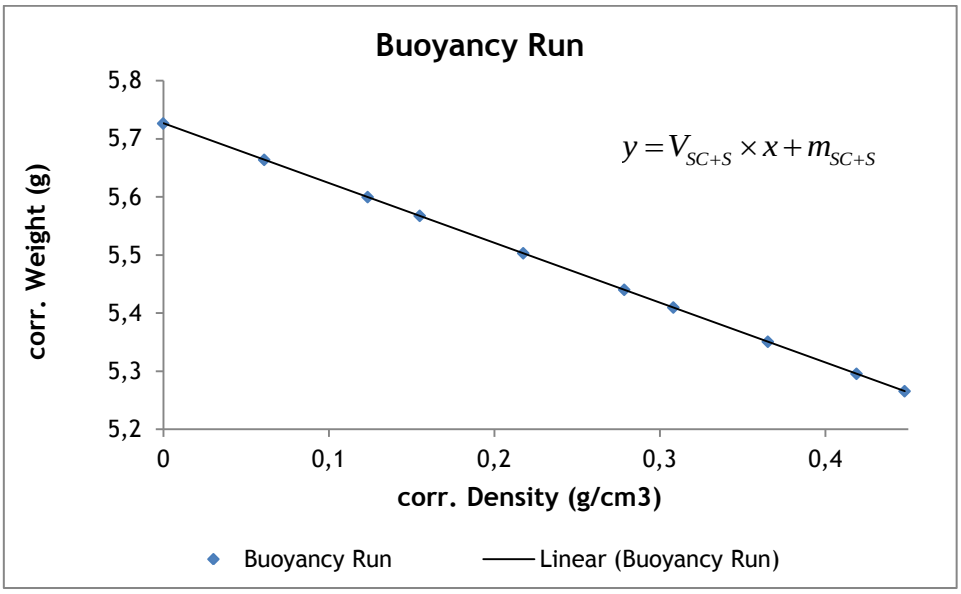

Figure 4.4 - Corrected weight as a function of corrected density

To obtain the desired values, m_S and V_S, real weight and volume of the sample, respectively, equations (4.4) and (4.5) are applied:.

$$m_S = m_{SC+S} - m_{SC} \tag{4.4}$$

Where m_{SC+S} is the mass of the sample container/sample system, and m_{SC} is the mass of the sample container.

$$V_S = V_{SC+S} - V_{SC} \tag{4.5}$$

Here V_{SC+S} is the volume of the sample container/sample system, and V_{SC} is the volume of the sample container.

The mass and the volume of the Sample Container were obtained previously through a blank measurement, done when the equipment was installed.

Measurement with Carbon Dioxide

From the moment when the pressure increases molecules of gas are adsorbed by the polymer, making it possible to obtain values for adsorbed gas mass as a function of the pressure. The mass of the adsorbed gas is given by the following equation:

$$m_{ads} = corr.Weight - m_{SC} - m_S + (V_{SC} + V_S) \times corr.Density \quad (4.6)$$

Where m_{ads} is the mass of the adsorbed gas, $corr.Weight$ is the weight (given by MSB in .equ file) and $corr.Density$ is the density value (corrected). The .equ file is where the MSB saves the values corresponding to equilibrium. These are the values to be treated; all the calculations are presented in Appendix 2 with more detail.

The uptake value is the ratio between the adsorbed gas mass in the polymer and the initial mass of the polymer, excluding any adsorbed gas. This value is presented in grams of gas per grams of polymer so that it can be easily compared with the literature:

$$S = \frac{m_{ads}}{m_S} \left[\frac{g_{gas}}{g_{polymer}} \right] \quad (4.7)$$

Absolute adsorption has to be calculated using a further correction. This correction accounts for the volume of adsorbed gas in the polymer.

The correction made to the absolute uptake consists in plotting the S as a function of $corr.Density$ and in calculating the negative slope, as seen in Figure 4.5. The negative slope corresponds to the volume of adsorbed gas in the polymer.

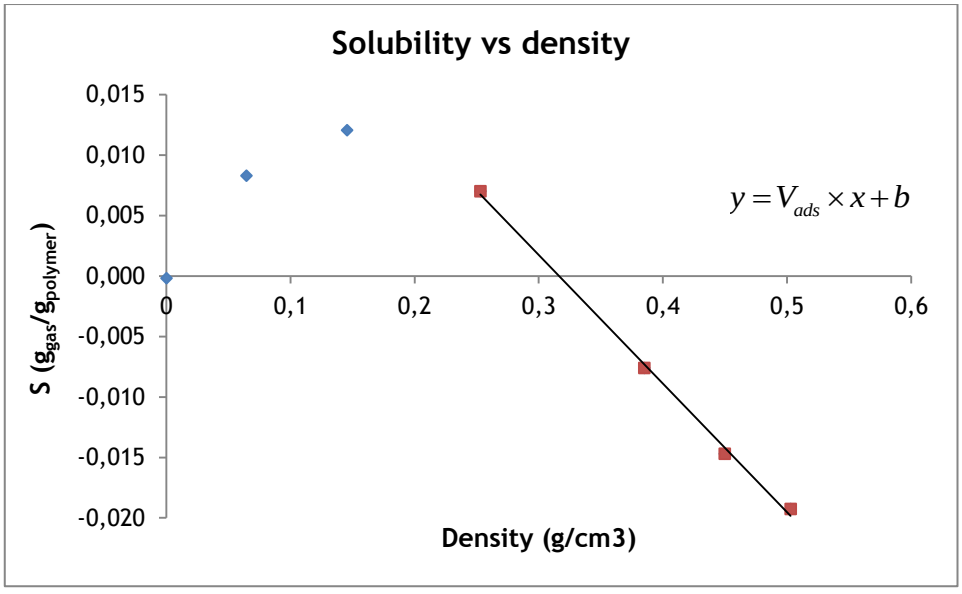

Figure 4.5 - Solubility of the penetrant as a function of Density to XLPE at 90°C up to 200 bar

Knowing the value of V_{ads}, the adsorbed gas, it is possible to calculate the absolute uptake:

$$S_{abs} = S + corr.Density \times V_{ads} \quad (4.8)$$

4.2 Experimental Results and Discussion

Experimental values are summarized in Table 4.2.

Table 4.2 - Solubility for each Pressure, Temperature and Polymer (average values)

Polymer	Pressure [bar]	Temperature [°C]	Solubility [$g_{gas}/g_{polymer}$]
PVDF	74.97	45.16	0.0545
	100.02	45.28	0.0545
	150.09	45.18	0.0772
	75.17	85.90	0.0275
	100.07	85.75	0.0340
	153.07	85.95	0.0375
XLPE	99.98	44.78	0.0430
	200.03	44.60	0.0974
	299.82	44.50	0.1087
	100.00	90.00	0.0320
	199.78	90.67	0.0343
	300.13	90.55	0.0440

The tests were conducted a number of times for each pressure and temperature in order to achieve consistent results. The mean values of these measurements are given in table 4.2, and figures 4.6 and 4.7 show curves of the solubility as a function of pressure for each of the individual measurements.

With PVDF it was not possible to reach the desired 90 °C because the equipment was not working properly, this measurement should be repeated to reach the desired temperature. All the results presented in this document will be presented to the real temperature (85 °C).

It was possible to conclude that the solubility increases with the increasing pressure. At 100 bar unusual behavior was observed: this happen because at this pressure the density of carbon dioxide is a strong function of pressure (see figure 3.2); 100 bar is near the critical pressure where the density becomes rather sensitive to pressure.

4.2.1 PVDF

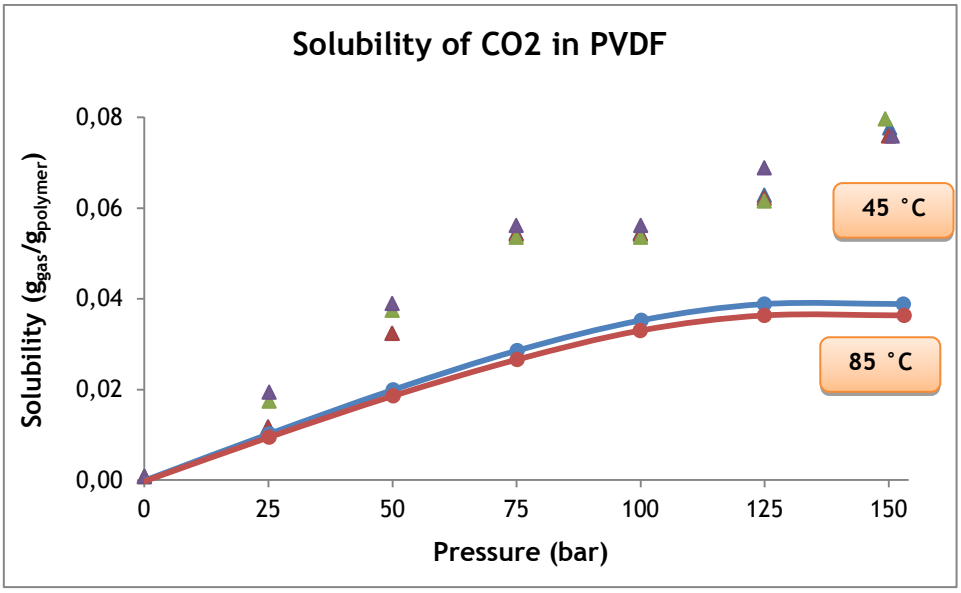

Figure 4.6 - Experimental results for solubility of Carbon Dioxide in PVDF at 45 °C and 90 °C. The dots represent the measurements at 45 °C and the lines with dots represent the measurements at 85 °C.

4.2.2 XLPE

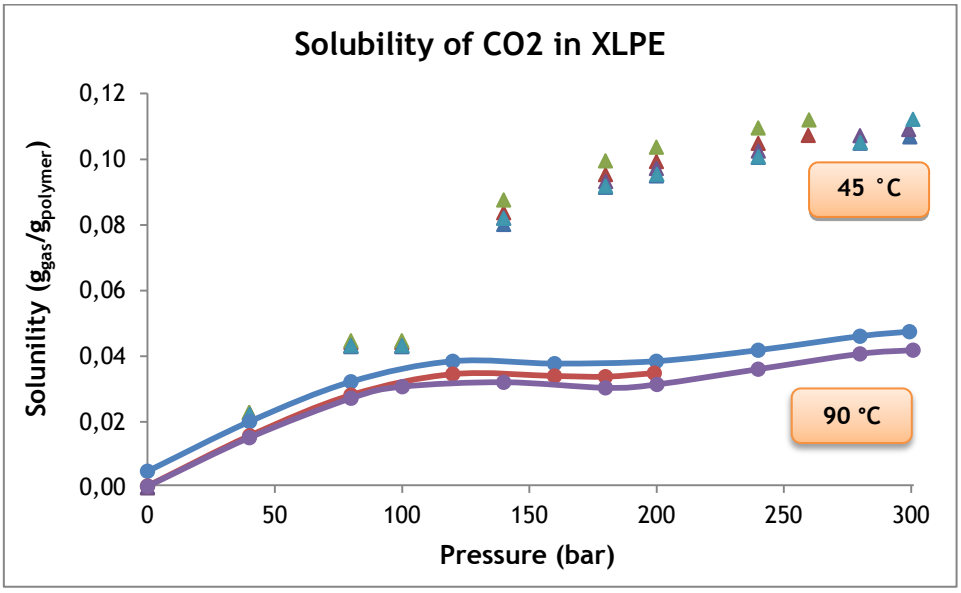

Figure 4.7 - Experimental results for solubility of Carbon Dioxide in XLPE at 45 °C and 90 °C. The dots represent the measurements at 45 °C and the lines with dots represent the measurements at 90 °C.

4.3 Modeling

The solubility of carbon dioxide in polymers was modeled with the sPC-SAFT equations of state. The average of experimental results were used to find the most suitable value of the binary interaction parameter, k_{ij} .

4.3.1 PVDF

Figures 4.8, 4.9 and 4.10 show the results with varying binary interaction parameters. No single binary parameter captures the effect of pressure – especially at 45 °C. However, depending on the expected operating pressure, the appropriate k_{ij} can be chosen.

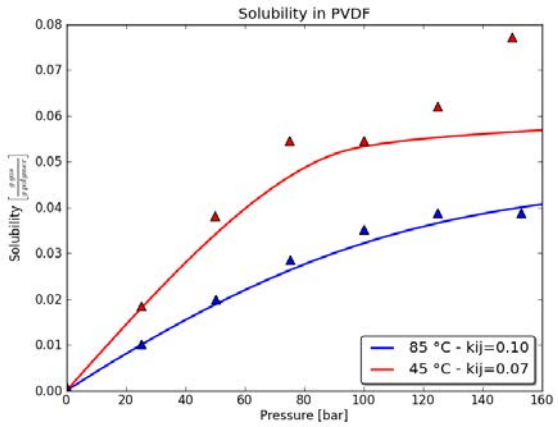

Figure 4.8 - sPC-SAFT solubility correlations for CO_2 in PVDF at 45 °C and 85 °C The binary parameter is selected to reproduce the lower pressure data. The dots are the average of experimental results.

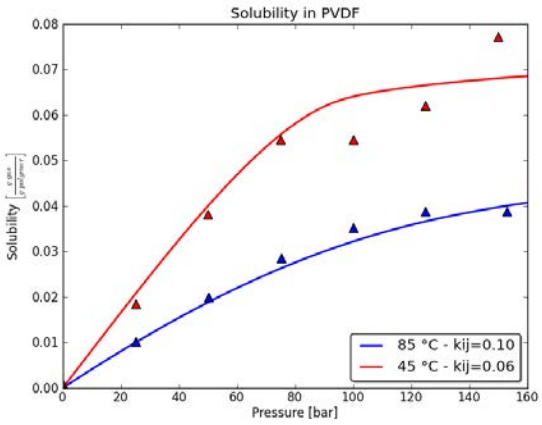

Figure 4.9 - sPC-SAFT solubility correlations for CO_2 in PVDF at 45 °C and 85 °C. The binary parameter is selected to reproduce the intermediate pressure data.. The dots are the average of experimental results.

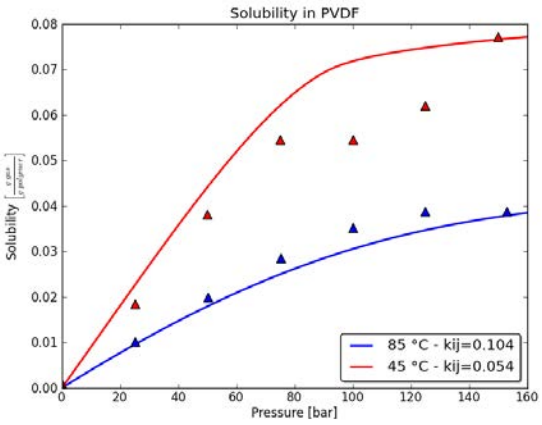

Figure 4.10 - sPC-SAFT solubility correlations for CO_2 in PVDF at 45 °C and 85 °C The binary parameter is selected to reproduce the highest pressure data.. The dots are the average of experimental results.

It is possible to conclude that, at 45 °C, the binary interaction parameter has an important influence in solubility, because small changes in this parameter cause large variations in the

solubility curve. At 85 °C, a single binary parameter reproduces the data well over the whole pressure range.

4.3.2 XLPE

Figures 4.11, 4.12 and 4.13 show the effect of the binary interaction parameter on solubility correlations for CO_2 in XLPE.

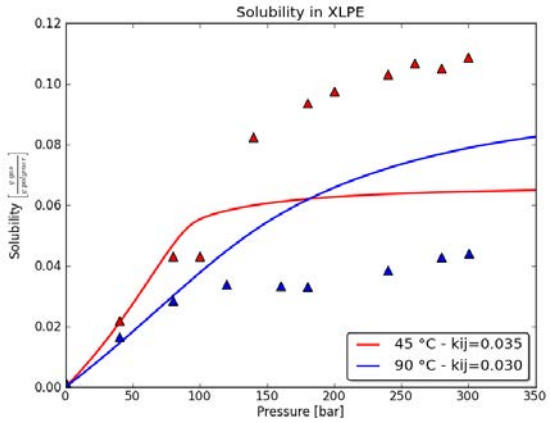

Figure 4.11 - sPC-SAFT correlations for solubility of CO_2 in XLPE at 45 °C and 90 °C. The binary parameter is chosen so that the model reproduces the low pressure data. The dots are the average of experimental results.

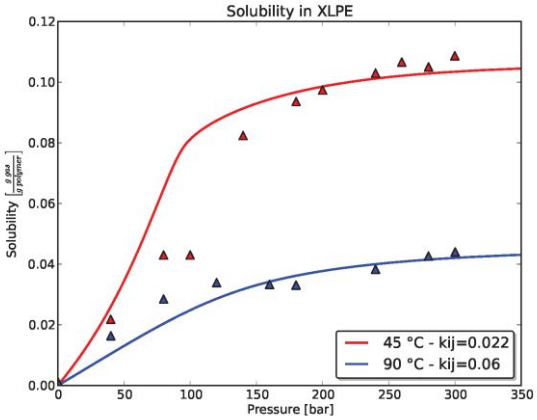

Figure 4.12 - sPC-SAFT correlations for solubility of CO_2 in XLPE at 45 °C and 90 °C. The binary parameter is chosen so that the model reproduces the intermediate pressure data. The dots are the average of experimental results

.

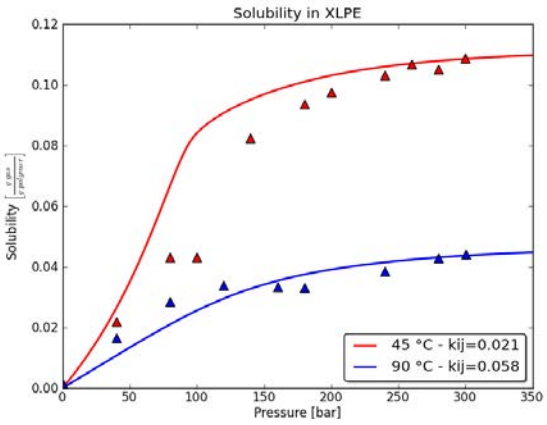

Figure 4.13 - sPC-SAFT correlations for solubility of CO_2 in XLPE at 45 °C and 90 °C,. The binary parameter is chosen so that the model reproduces the high pressure data.. The dots are the average of experimental results.

At both temperatures if the k_{ij} is selected to reproduce the low pressure data, the errors at intermediate and high pressure are significant. However if the k_{ij} is chosen to reproduce the intermediate and high pressure data, the errors at low pressure are not that significant. Therefore it was concluded that the binary interaction parameter, k_{ij} , correlated to intermediate pressure data is an acceptable value to represent the solubility of carbon dioxide in XLPE over the whole pressure range.

4.4 Influence of Temperature

In order to study the influence of the temperature on solubility, and determine the parameters of the Arrhenius Equations, the Logarithm of the solubility as a function of inverse temperature was plotted. For each pressure, four plots were made: the experimental solubility, model at the lower pressure, model at the intermediate pressure and model at the upper pressure. All this plots are presented in Appendix 4. The solubility values and the calculated parameters were compared. The van't Hoff Equation is linearized as:

$$S = P_0 \exp\left(\frac{-\Delta H_S}{RT}\right) \Leftrightarrow \ln(S) = \ln(S_0) - \frac{\Delta H_S}{R} \times \frac{1}{T}$$

The slope of the line corresponds to $-\Delta H_S / R$, so the value of ΔH_S can be determined, the heat of dissolution of a penetrant mole in the matrix. The ordinate corresponds to $\ln(S_0)$, so the value of S_0 can be found. This represents the limiting value of solubility for infinite molecular agitation $T \to \infty$.

Table 4.3 - The pre-exponential term in the Arrhenius equation for solubility. The results are for the solubility measured from the experimental work and modeled to reproduce the lower, intermediate and upper pressures.

	S_0			
Pressure (bar)	Experimental	Lower	Intermediate	Upper
75	2.19×10^{-4}	4.01×10^{-4}	1.17×10^{-4}	3.69×10^{-5}
100	1.22×10^{-3}	8.68×10^{-4}	2.38×10^{-4}	6.98×10^{-5}
150	2.28×10^{-4}	3.52×10^{-3}	9.39×10^{-4}	2.64×10^{-4}

Table 4.4 - Heat of dissolution of a penetrant mole in the matrix in the Arrhenius equation for solubility. The results are for the measured solubility modeled solubility for the lower, intermediate and upper pressures. Literature values are also presented.

	ΔH_S (kJ/mol)				
Pressure (bar)	Experimental	Lower	Intermediate	Upper	Flaconnèche et al. (2001)
75	-14.596	-12.583	-16.307	-19.645	Between -20 and -10
100	-10.052	-10.891	-14.796	-18.346	
150	-15.408	-7.334	-11.327	-14.992	

Once more the experimental results at 100 bar show an unusual behavior compared with the results at 75 bar and 150 bar. This behavior is observed in figure A4.1, when the experimental point at 100 bar and 45 °C match the one at 75 bar for the same temperature.

The values for ΔH_S agree with the literature, although the reported values in literature are for 40 bar. The values of ΔH_S for the experimental results of solubility for 75 bar concur with the model values for modeled solubility respecting low pressures, for 100 bar concur with the model values for solubility respecting mean pressures and at 150 bar concur with the model values for solubility respecting upper pressures. This is not surprising since the model was fitted to the experimental results at each condition,

Table 4.5 - Results of the pre-exponential term in the Arrhenius equation for solubility. The results are for the solubility from the experimental work and modeled respecting the lower, intermediate and upper pressures.

	S_0			
Pressure (bar)	**Experimental**	**Lower**	**Intermediate**	**Upper**
100	3.97×10^{-3}	2.54×10^{-3}	7.15×10^{-6}	4.46×10^{-6}
200	2.11×10^{-5}	9.25×10^{-2}	4.24×10^{-5}	4.07×10^{-5}
300	7.37×10^{-5}	3.25×10^{-1}	7.33×10^{-5}	6.92×10^{-5}

Table 4.6 - Results of the heat of dissolution of a penetrant mole in the matrix in the Arrhenius equation for solubility. The results are for the solubility from the experimental work and modeled respecting the lower, intermediate and upper pressures.

	ΔH_S (kJ/mol)			
Pressure (bar)	**Experimental**	**Lower**	**Intermediate**	**Upper**
100	-6.305	-8.139	-24.698	-26.037
200	-22.311	1.032	-20.501	-20.730
300	-19.298	4.280	-19.180	-19.461

Is not possible to compare the results with literature since no results were found. Comparing the results of S_0 and ΔH_S to the modeled values with respect to the intermediate and the upper pressures we can conclude that they are quite similar.

5 Permeability Experiments

5.1 Experimental work

5.1.1 Equipment

The permeability is obtained in a 2-D permeation cell. The high pressure 2-D permeation cell was designed and manufactured by the Department of Chemical and Biochemical Engineering at Technical University of Denmark. The operating conditions of the cell are up to 150 °C and 700 bar absolute. The cell consists of two stainless steel chambers: a high-pressure chamber – or primary chamber – and a low pressure chamber – or secondary chamber. The set-up of the equipment is shown in Figure 5.2.

The polymer sample is placed between the two chambers; it is a disc about 10 cm in diameter and 1-2 mm thick. The two chambers are supported by two porous plates to prevent the sagging of the polymer sample during the measurement. These plates are porous to allow gas to freely contact the sample. The low pressure chamber has a free internal volume of 22.057 cm^3 and the high pressure chamber has a variable volume to the metal below placed inside the chamber. The volume of the high pressure chamber varies by injection or removal of water using an ISCO high pressure water pump. The two chambers are held together by two stainless steel flanges, these flanges are securely fastened by the use of 8 heavy-duty stud bolts. The entire cell, after assembly, is mounted on a hook on a frame in the fume hood. In Figure 5.1 shows the entire cell prepared for an experiment.

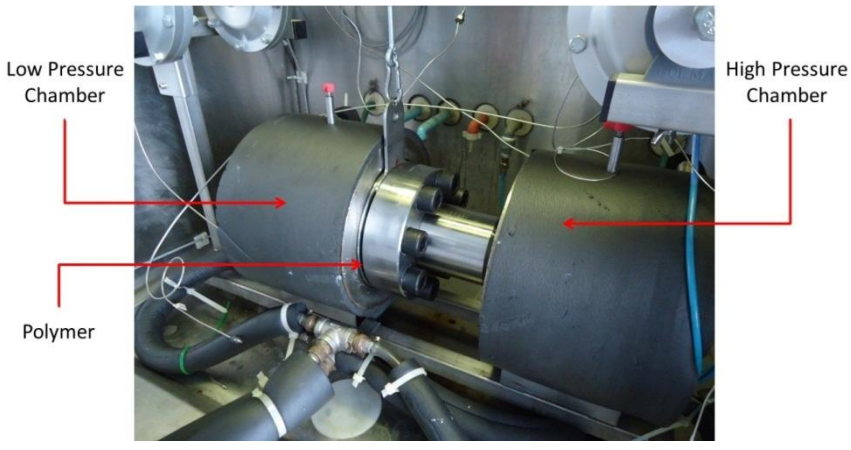

Figure 5.1 - Permeation Cell assembled prior to a run

During the procedure it is possible to measure the temperature with a Pt-100 thermocouple placed between the high-pressure and the low-pressure chambers, next to polymer. The temperature in the chambers is controlled by circulating hot glycerin in two

heating jackets surrounding both chambers. The pressure in the chambers is measured by two Fisher-Rosemount pressure transducers.

A computer program developed in-house is used to collect the data from measurements (temperature and pressure as function of the time).

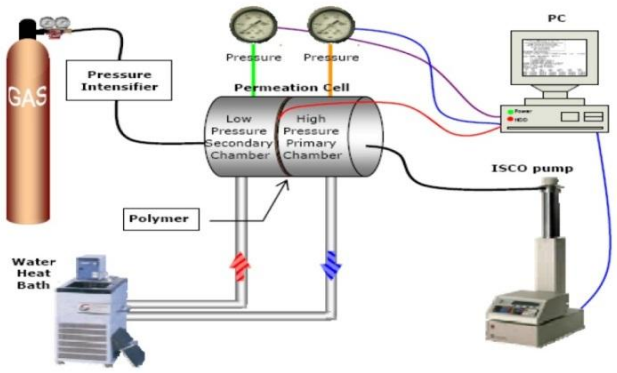

Figure 5.2 - Schematic set-up of high-pressure 2-D permeation cell

5.1.2 Experiments Performed

Tests were performed with the two polymers referred to previously (PVDF and XLPE).

Permeability was measured according to the temperature and pressure conditions presented in Table 5.1.

Table 5.1 - Conditions for the permeability experiments

	Temperature (°C)			
$P_{High\ Pressure\ Chamber}$ (bar)	45	60	75	90
100	●□	□	□	□

Here ● corresponds to the test performed with PVDF and □ to the tests performed with XLPE. Pure carbon dioxide was used in all experiments.

5.1.3 Experimental procedure

One disk of polymer, approximately 10 cm in diameter, was cut and placed between the high and low pressure chambers. The heating jackets are positioned surrounding the cell; these jackets prevent heat losses to the environment. The circulation of heating fluid is initiated to start heating up the system to the desired temperature.

Before starting the measurement with gas, the cell was evacuated from both chambers, for this vacuum is applied to the entire cell for approximately one day. The evacuation serves to remove all the dissolved gases in the polymer.

The CO_2 is loaded by opening valves to the high pressure chamber and to the low pressure chamber. The high pressure chamber is loaded until the desired pressure is attained and the low pressure chamber is loaded until a pressure difference of 55 bar between the high and low pressure side is reached. After some time it can be observed that the pressure in the low pressure chamber increases, this is a consequence of the gas permeation. However, the pressure in the high pressure chamber is maintained constant. The pressures in both chambers are recorded as a function of the time, as well as the temperature and the amount of water lost to keep the pressure. Using the characteristics of the sample and the low pressure data it is possible to determine the diffusivity and the permeability.

5.1.4 Calculation method

Diffusivity

For the calculation of diffusion the direct applications of the concepts described in the theory were used. When the curve described in figure 3.4 is observed, the equation (3.7) can be applied to obtain the diffusion coefficient.

Permeability

The permeability is calculated using equation (3.13).

5.2 Experimental Results and Discussion

5.2.1 PVDF

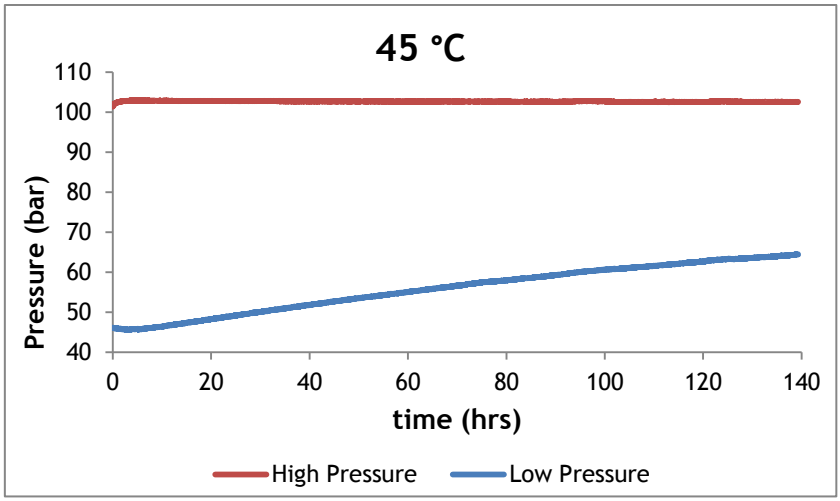

Figure 5.3 - Pressure in High Pressure and in Low Pressure Chamber for PVDF at 45 °C.

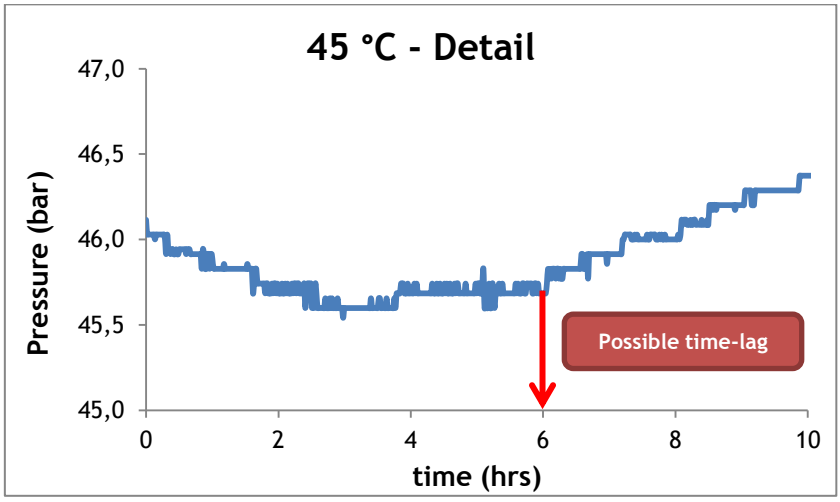

Figure 5.4 - Detail of measurement with PVDF at 45 °C with high pressure chamber at 100 bar.

As the experiment was not repeated is not possible to admit that this value is the time-lag, and so, is not possible to determine the diffusion coefficient.

Table 5.2 - Results of Permeability and Diffusion through PVDF at $P_{\text{High Pressure Chamber}}$ = 100 bar and 45 °C

$P_{\text{High Pressure Chamber}}$ = 100 bar	
Temperature (°C)	45
Pe $\times 10^{-7}$ [cm^3 STP/(cm·bar·s)]	0.791

5.2.2 XLPE

$P_{High\ Pressure\ Chamber}$ = 100 bar

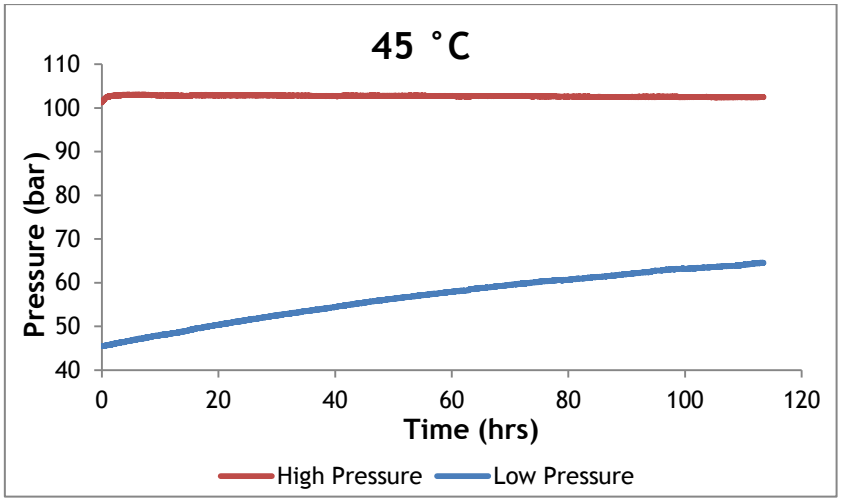

Figure 5.5 - Pressure in High Pressure and in Low Pressure Chamber for XLPE at 45 °C.

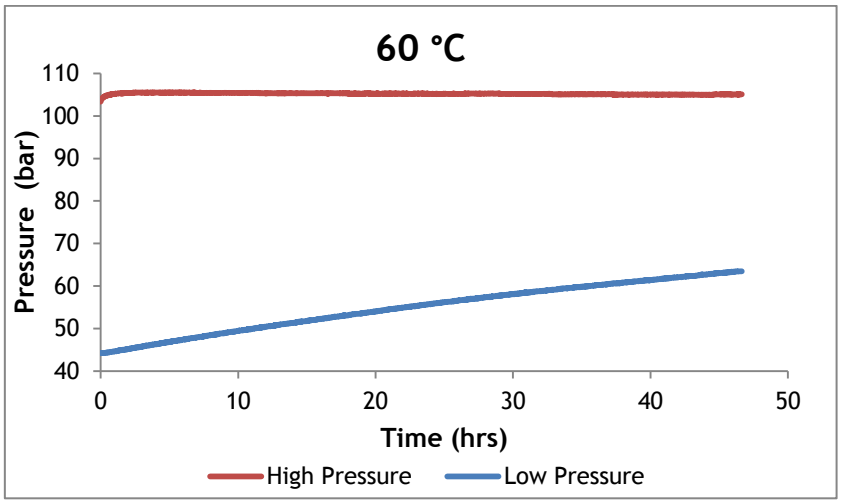

Figure 5.6 - Pressure in High Pressure and in Low Pressure Chamber for XLPE at 60 °C.

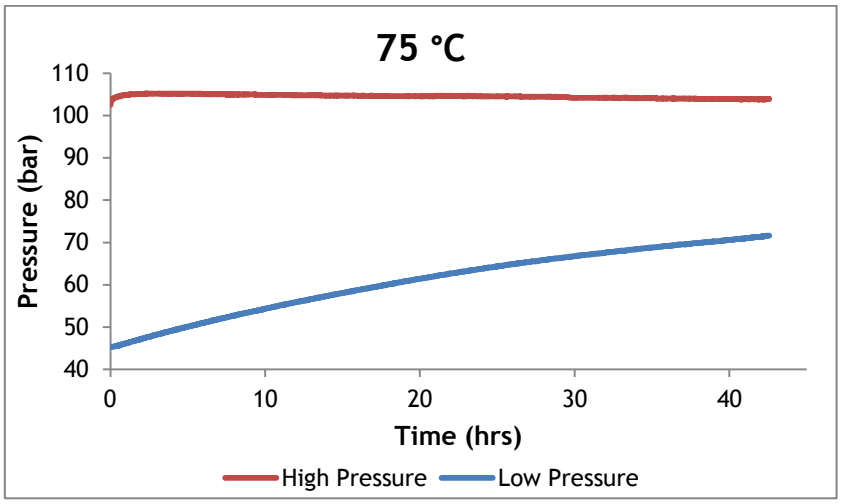

Figure 5.7 - Pressure in High Pressure and in Low Pressure Chamber for XLPE at 75 °C.

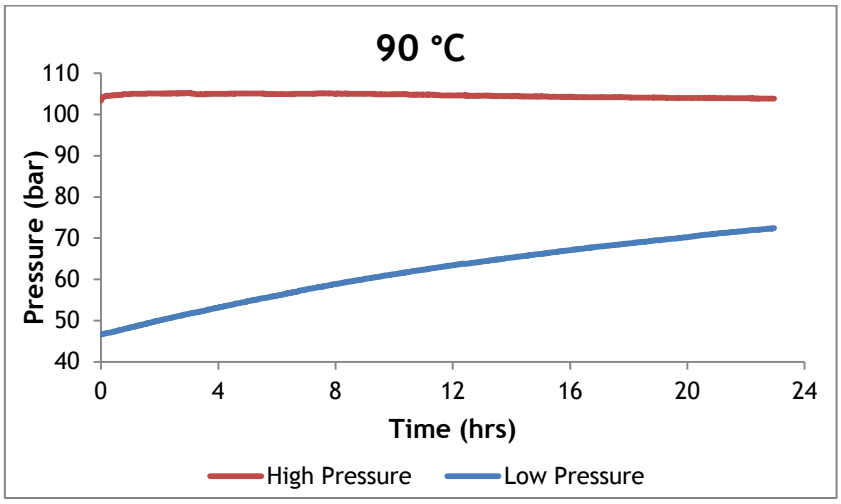

Figure 5.8 - Pressure in High Pressure and in Low Pressure Chamber for XLPE at 90 °C.

The experiment started with approximately 45 bar in the low pressure chamber and 100 bar in the high pressure chamber. The pressure in the high pressure chamber was kept constant and the pressure in low pressure chamber increases with time, this reflects the passage of the gas through the polymer membrane. At higher temperatures the pressure increase is faster since the permeability increases with increasing temperature, as discussed in the theory section earlier.

With XLPE is not possible to observe the time-lag in the beginning of the measurement, so it is not possible to calculate the diffusion by this method.

Table 5.3 - Results for Permeability through XLPE at $P_{High\ Pressure\ Chamber}$ = 100 bar to 45, 60, 75 and 90 °C

$P_{High\ Pressure\ Chamber}$ = 100 bar				
Temperature (°C)	45	60	75	90
Pe $\times 10^{-7}$ [cm^3 STP/(cm·bar·s)]	1.199	1.788	2.832	4.642

5.3 Influence of Temperature

5.3.1 XLPE

In order to study the influence of the temperature on permeability, and determine the parameters of the Arrhenius Equations, the Logarithm of the solubility as a function of inverse temperature was plotted. The influence of permeability was studied just for XLPE and for pressure in high pressure chamber of 100 bar; the plot is presented in Appendix 5. The Arrhenius Equation is linearized as:

$$Pe = Pe_0 \exp\left(\frac{-E_P}{RT}\right) \Leftrightarrow \ln(Pe) = \ln(Pe_0) - \frac{E_P}{R} \times \frac{1}{T}$$

The slope of the line corresponds to E_P/R, so the value of E_P can be determined, the apparent activation energy for permeation process. The ordinate corresponds to $\ln(Pe_0)$, so the value of Pe_0 can be found. This represents the limiting value of permeability for infinite molecular agitation $T \to \infty$.

$\ln(Pe_0)$	$Pe_0 \times 10^{-3}$ (exp)	E_P/R	E_P (exp)
-4.713	8.98	-3588.3	-29.8331 Kj/mol

It is not possible to compare these results with the literature since no experiments have been reported with this polymer.

6 Conclusions

The Magnetic Suspension Balance experimental set-up was well suited for measuring the solubility of supercritical carbon dioxide in polymers. By observing the values of the solubility for both polymers it is possible to conclude that the difference of solubility between them is not so significant. The solubility increases with the increasing of pressure but decreases with increasing temperature. An unusual behavior of the tendency of solubility at 100 bar was observed. This effect could be related with the jump of carbon dioxide density.

It was possible to model the experimental results using the sPC-SAFT equations of state. Three models were made for both polymers at each temperature. But it was observed that, for lower pressure and pressure near the critical point, the model was not so consistent. So it is assumed that the model for intermediate pressure presents the most acceptable values for k_{ij} (binary interaction parameter).

In the study of the influence of temperature in the solubility, the obtained parameters were in agreement with the results found in the literature.

The high pressure 2-D permeation cell set-up was well suited for measuring the permeability of supercritical carbon dioxide in polymers. Although the equipment was not working as expected, keeping the pressure difference between both chambers, it was possible to calculate the permeability of the gas in polymers using the average of the difference between chambers. The value of the diffusion coefficient obtained by time-lag method could not be very accurate.

7 List of References

Adewole, J., Jensen, L., Al-Mubaiyedh, U., von Solms, N., & Hussein, I. (2012). Transport properties of natural gas through polyethylene nanocomposites at high temperature and pressure. *J. Polym. Res.19, pp9814*

Andreasen, M., Frederiksen, K., von Solms, N., Kristensen, J., & Neela, V. (2008). *Polymerer i anlæg med CO2 som kølemiddel*. internal report

Braand, P., & Procida, I. (2012). *Patent No. US 8, 163, 364, B2*. Denmark.

Callister, W. (2007). *Materials Science and Engineering - An Introdution*. John Wiley & Sons, Inc.

Costello, L., & Koros, W. (1992). Temperature dependence os gas sorption and transport properties in polymers: measurement ans applications. *Ind. Eng. Chem. Res., 31*, pp. 2708-2714.

Dandekar, A., Lindeloff, N., Andersen, S., Jakobsen, E., & Stenby, E. (2000). Measurement of Gas Transport Properties in Polymers using a High-Pressure Flat Geometry Permeation Cell. internal report

Dreisbach, F., Lösch, H., & Harting, P. (2002). Highest Pressure Adsorption Equilibria Data: Measurement with Magnetic Suspension Balance and Analysis with a New Adsorbent/Adsorbate-Volume. *Adsorption, 8*, pp. 95-109.

Flaconnèche, B., Martin, J., & Klopffer, M. (2001). Permeability, Diffusion and Solubility of Gases in Polyethylene, Polyamide 11 and Poly(vinylidene fluoride). *Oil & Gas Science and Technology, 56*, pp. 261-278.

Flaconnèche, B., Martin, J., & Klopffer, M. (2001). Transport Properties os Gases in Polymers: Experimental Methods. *Oil & Gas Science and Technology, 56*, 245-259.

Frisch, H. (1980). Sorption and Transport in Glassy Polymers - A Review. *Polymers Engineering and Science, 20*.

Grenner, A., Kontogeorgis, G., von Solms, N., & Michelsen, M. (2007). Modeling phase equilibria of alkanols with the simplified PC-SAFT equations of state and generalized pure compound parameters. *Fluid Phase Equilibria, 258*, pp. 83-94.

Gross, J., & Sadowski, G. (2001). Perturbed-Chain SAFT: An Equation of State Based on a Perturbation Theory for Chain Molecules. *Ind. Eng. Chem. Res., 40*, 1244-1260.

Klopffer, M., & Flaconnèche, B. (2001). Transport Properties os Gases in Polymers: Bibliographic Review. *Oil & Gas Science ans Tecnology, 56*, 223-244.

Kouskoumvekaki, I., von Solms, N., Lindvig, T., Michelsen, M., & Kontogeorgis, G. (2004). Novel Method For Estimating Pure-Component Parameters for Polymers: Application to the PC-SAFT Equation of State. *Ind. Eng. Chem. Res., 43*, 2830-2838.

Lin, H., & Freeman, B. (2004). Gas solubility, diffusivity and permeability in poly(ethylene oxide). *Journal of Membrane Science, 239*, pp. 105-117.

Lundsgaard, R. (2011). Modeling Solubility and Swelling in Supercritical Carbon Dioxide – Polymer Systems, internal report *CERE 1218*

Moellmer, J., Moeller, A., Dreisbach, F., Glaeser, R., & Staudt, R. (2011). High pressure adsorption of hydrogen, nitrogen, carbon dioxide and methane on the metal-organic framework HKUST-1. *Microporous and Mesoporous Materials, 138*, pp. 140-148.

Nalawade, S., Picchioni, F., & Janssen, L. (2006). Supercritical carbon dioxide as green solvent for processing polymer melts: processing aspects and applications. *Prog. Polym. Sci, 31*, pp. 19-43.

Neela, V., & von Solms, N. (2008.). Refrigeration plants using Carbon Dioxide as Refrigerant: measuring and modeling the permeability, diffusivity and solubility of carbon dioxide in polymers used as packing and sealing materials, *internal report CERE 0812*.

Neergaard, J., Hassager, O., & Szabo, P. (2003). Molecular Model for Solubility of Gases in Flexible Polymers. *Inc. J Polym Sci Part B: Polym Phys, 41*, pp. 701-706.

Nielsen, J. (2001). *Permeation and solubility experiments performed at DTU*. DTU, Department of Chemical Engineering. internal report

Pini, R., Ottiger, S., Rajendran, A., Storti, G., & Mazzotti, M. (2006). Reliable Measurement of near-critical adsorption by gravimetric method. *Adsorption, 12*, pp. 393-403.

Procida, I., & Rishøj Nielsen, N. (2007). Inline IR-Cured XLPE Technology for Flexible Pipes. *Offshore Technology Conference*. Houston.

Rubin, A., & Wang, C. (2012). Qualification of Flexible Dynamic Risers for Supercrtitica CO2. *Offshore Technology Conference*. Houston.

Rubotherm (Präzisionsmeßtechnik GmbH). (2009). *Operating Procedure - Gravimetric Adsorption Measurements*. Bochum - Germany.

Sameer. (2006). Supercritical carbon dioxide as a green solvent for processing polymer melts: Processing aspects and applications. *Prog. Polym. Sci., 31*, 19-43.

Union Engineering. (n.d.). Properties of Carbon Dioxide. Fredericia, Denmark.

von Solms, N., & Andersen, S. (2004). *Final Report: Samarbejdsprojekt mellem IVC-SEP og NKT Flexibles A/S.* internal report

von Solms, N., & Kristensen, J. (2010). Refrigeration plants using carbon dioxide as refrigerant: measuring and modelling the solubility and diffusion of carbon dioxide in polymers used as sealing materials. *International Journal of Refrigeration, 33*, pp. 19-25.

von Solms, N., Kouskoumvekaki, I., Michelsen, M., & Kontogeorgis, G. (2006). Capabilities, limitations and challenges of simplified PC-SAFT equations of state. *Fluid Phase Equilibria, 241*, 344-353.

von Solms, N., Michelsen, M., & Kontogeorgis, G. (2003). Computational and Physical Performance of a Modified PC-SAFT Equation of State for Highly Asymmetric and Associating Mixtures. *Ind. Eng. Chem. Res., 42*, 1098-1105.

von Solms, N., Michelsen, M., & Kontogeorgis, G. (2005). Prediction and Correlation of High-Pressure Gas Solubility in Polymers with Simplified PC-SAFT. *Ind. Eng. Chem. Res., 44*, 3330-3335.

von Solms, N., Nielsen, J., Hassager, O., Rubin, A., Dandekar, A., Andersen, S., et al. (2004). Direct measurement of gas solubilities in polymers with a high-pressure microbalance. *Journal of Applied Polymer Science, 91*, pp. 1476-1488.

von Solms, N., Rubin, A., Andersen, S., & Stenby, E. (2005)). Directs measurements of high temperature/high pressure solubility of methane and carbon dioxide in Polyamide (PA-11) using a high-pressure microbalance. *International Journal of Thermophysics, 26* pp. 115-125

von Solms, N., Zecchin, N., Rubin, A., Andersen, S., & Stenby, E. (2005). Direct measurement of gas solubility and diffusity in poly(vinylidene fluoride) with a high-pressure microbalence. *European Polymer Journal, 41*, pp. 341-348.

http://webbook.nist.gov/chemistry/ , April – June 2012

http://www.doitpoms.ac.uk/tlplib/polymerbasics/crystallinity.php ,June 2012

Appendix 1 – sPC-SAFT Equations

The starting point is the most general form of the Helmholtz energy for a mixture of associating molecules.

$$\tilde{a} \equiv \frac{A}{NkT} = \tilde{a}^{id} + \tilde{a}^{hc} + \tilde{a}^{disp} + \tilde{a}^{assoc} \tag{A1.1}$$

Where $\tilde{a}^{id}$ is the ideal gas contribution, $\tilde{a}^{hc}$ is the contribution of the hard-sphere chain reference system, $\tilde{a}^{disp}$ is the dispersion contribution arising from the square-well attractive potential and $\tilde{a}^{assoc}$ is the contribution due to association.

The expressions for the contributions from the ideal gas ($\tilde{a}^{id}$) and dispersion ($\tilde{a}^{disp}$) are from Gross and Sadowski (2001).

The contribution to the hard-chain term is made up the two contributions: the hard-sphere term and chain formation term,

$$\tilde{a}^{hc} = \bar{m}\tilde{a}^{hs} - \sum_i x_i \left(m_i - 1\right) \ln g_{ii}^{hc}\left(d_{ii}^{+}\right) \tag{A1.2}$$

Where $\bar{m}$ is a mean segment length defined simply as $\bar{m} = \sum_i x_i m_i$ and the hard-sphere term is given by:

$$\tilde{a}^{hs} = \frac{4\eta - 3\eta^2}{\left(1-\eta\right)^2} \tag{A1.3}$$

Where x_i is the mole fraction of component i. The radial distribution function at contact is:

$$g^{hs}\left(d^{+}\right) = \frac{1-\eta/2}{\left(1-\eta\right)^3} \tag{A1.4}$$

The equations (A1.3) and (A1.4) constitute modification 2 proposed by von Solms et al. (2003). The volume fraction $\eta = \pi\rho\bar{m}d^3/6$ is based on the diameter of an equivalent one-component mixture

$$d = \left(\frac{\sum_i x_i m_i d_i^3}{\sum_i x_i m_i} \right)^{1/3} \tag{A1.5}$$

Where the individual d_i are temperature-dependent segment diameters

$$d_i = \sigma_i \left[1 - 0{,}12 \exp\left(-3 \left(\frac{\varepsilon_i}{kT} \right) \right) \right] \tag{A1.6}$$

Appendix 2 – Calculation Example for solubility

Polymer: XLPE

Temperature: 90 °C

Measurement with Reference gas (Argon)

Tabela A2.1 - Data obtain with argon measurement at equilibrium

Segment	Temperature (°C)	Pressure (bar)	Corr.Weight (g)	Density (g/cm^3)	Corr.Density (g/cm^3)
1	86.3	0.04	5.7467	-0.0003	0.000
2	87.4	20.00	5.7190	0.0260	0.0263
3	87.6	39.96	5.6912	0.0524	0.0527
4	87.7	59.96	5.6633	0.0789	0.0792
5	87.8	79.97	5.6353	0.1053	0.1057
6	87.8	100.02	5.6074	0.1317	0.1321
7	87.9	119.96	5.5799	0.1578	0.1582
8	87.9	139.98	5.5524	0.1837	0.1841
9	88.0	159.98	5.5253	0.2093	0.2096
10	88.0	179.97	5.4986	0.2345	0.2348
11	88.0	189.97	5.4854	0.2469	0.2472
12	88.2	201.24	5.4717	0.2599	0.2602

$$Corr.Density_i = Density_i + 0.003 \quad \text{(A2.1)}$$

$$Corr.Density_1 = -0.0003 + 0.0003 = 0\ g/cm^3$$

$$Corr.Density_2 = 0.0260 + 0.0003 = 0.0263\ g/cm^3$$

(Same procedure for the other segments)

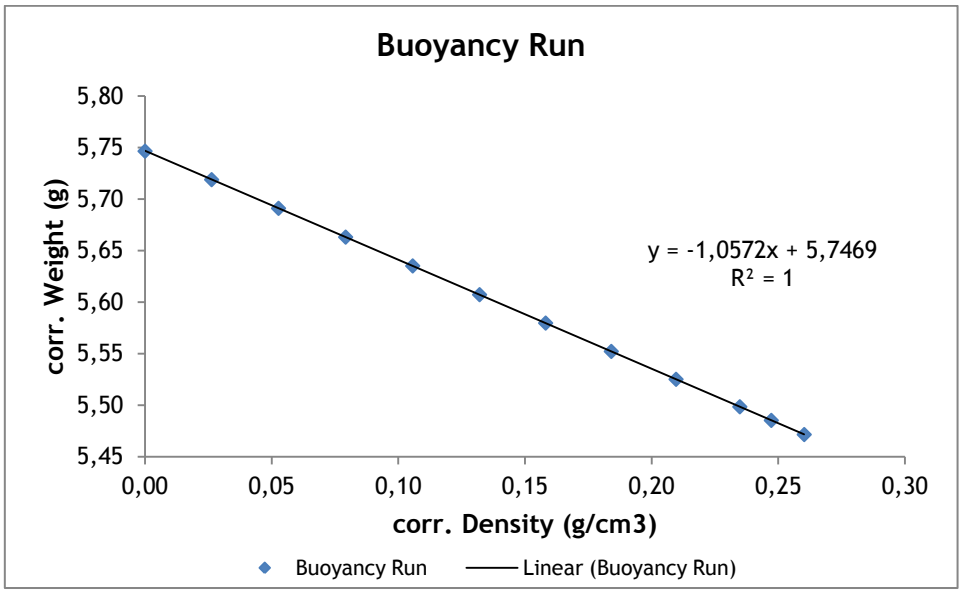

Figure A2.1 - Measurement with Argon to obtain the real weigh and volume of the sample

$m_{SC+S} = 5.7469\ g$ $V_{SC+S} = 1.0572\ cm^3$

$m_{SC} = 5.3917\ g$ $V_{SC} = 0.6790\ cm^3$

$m_S = 0.3517\ g$ $V_S = 0.3782\ cm^3$

Measurement with Carbon Dioxide

Tabela A2.2 - Data obtain with carbon dioxide measurement at equilibrium

Segment	Temperature (°C)	Pressure (bar)	Corr.Weight (g)	Density (g/cm^3)
1	84.2	0.05	5.7468	-0.0004
2	89.7	40.18	5.6817	0.0641
3	90.2	79.97	5.5973	0.1452
4	90.4	119.97	5.4820	0.2526
5	90.5	159.97	5.3372	0.3846
6	90.5	179.97	5.2662	0.4495
7	90.5	199.17	5.2084	0.5026

Tabela A2.3 - Results of calculations to obtain the absolute solubility

Segment	Corr.Density (g/cm^3)	$m_{adsorped}$ (g)	Solubility ($g_{gas}/g_{polymer}$)	Solubility $_{abs}$ ($g_{gas}/g_{polymer}$)
1	0.0000	-0.0001	-0.0002	-0.0002
2	0.0644	0.0029	0.0083	0.0151
3	0.1455	0.0042	0.0121	0.0275
4	0.2529	0.0025	0.0070	0.0339
5	0.3850	-0.0027	-0.0076	0.0333
6	0.4498	-0.0052	-0.0147	0.0331
7	0.5030	-0.0068	-0.0193	0.0342

$$m_{ads\_1} = 5.7468 - 5.3917 - 0.3517 + (0.6790 + 0.3782) \times 0 = -0.0001\,\text{g}$$

$$m_{ads\_2} = 5.6817 - 5.3917 - 0.3517 + (0.6790 + 0.3782) \times 0.0644 = 0.0083\,\text{g}$$

(Same procedure for the other segments)

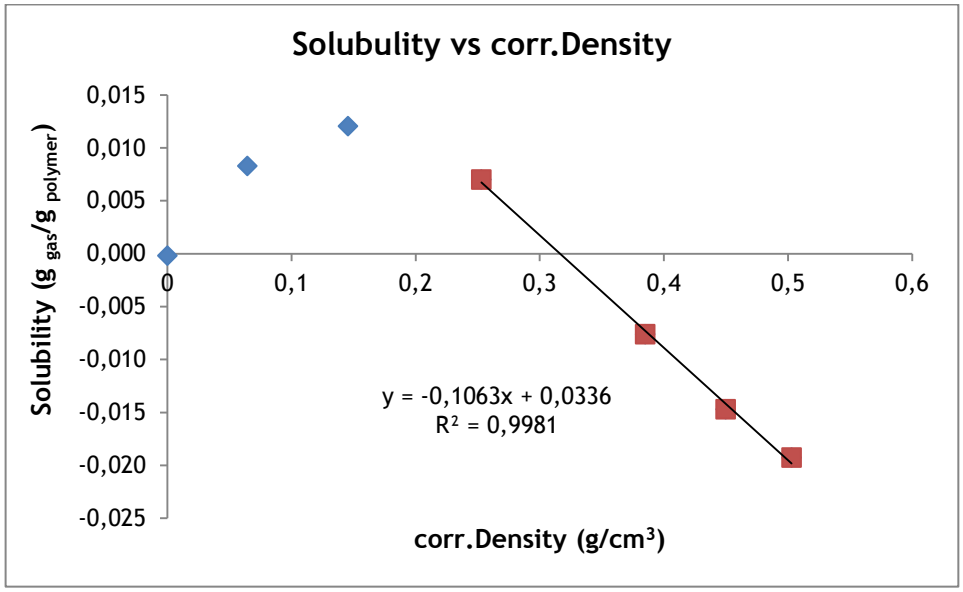

Figure A2.2 - Solubility of the penetrant as function of Density to XLPE at 90 °C up to 200 bar

$$V_{ads} = 0.1063\,cm^3/g$$

$$Solubility\ abs_1 = -0.0002 + 0 \times 0.1063 = -0.0002\ g_{gas}/g_{polymer}$$

$$Solubility\ abs_{2} = 0.0083 + 0.0644 \times 0.1063 = 0.0151\, g_{gas} / g_{polymer}$$

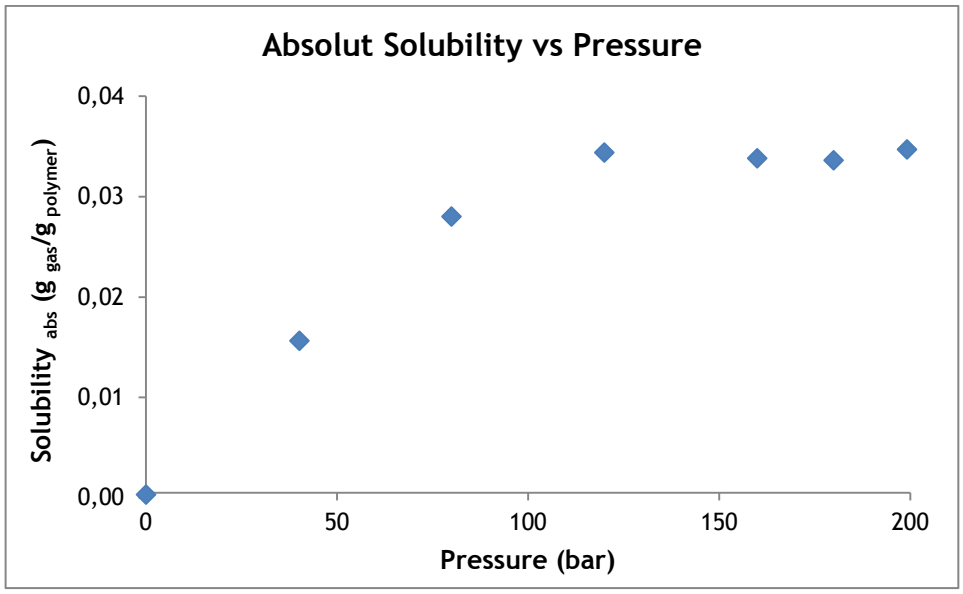

Figure A2.3 - Experimental results for Absolute solubility of Carbon Dioxide in XLPE at 90 °C

Appendix 3 - Influence of Temperature Graphs in Solubility

- **PVDF**

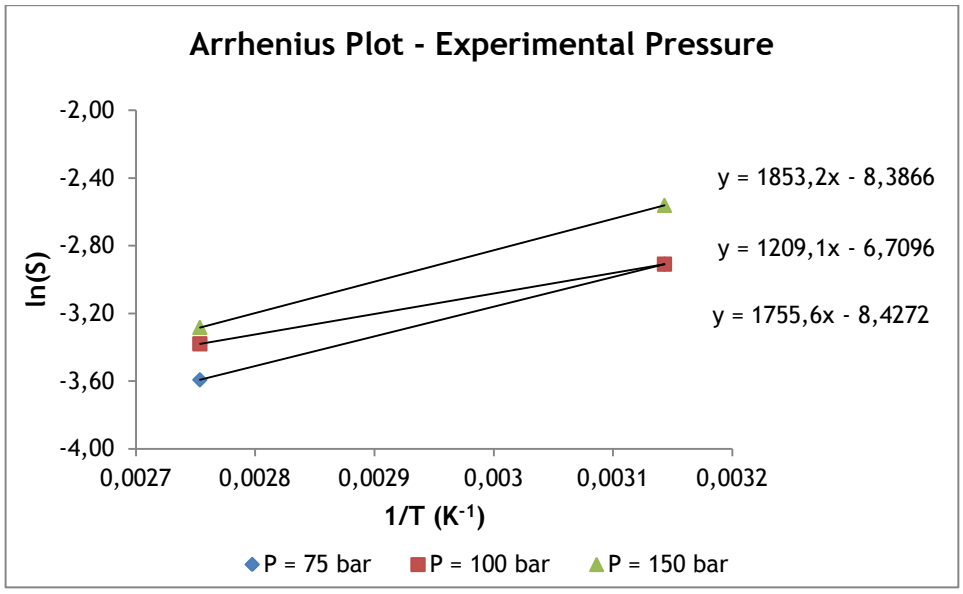

Figure A3.1 - Arrhenius plot for experimental solubility of CO_2 at three pressures, in PVDF.

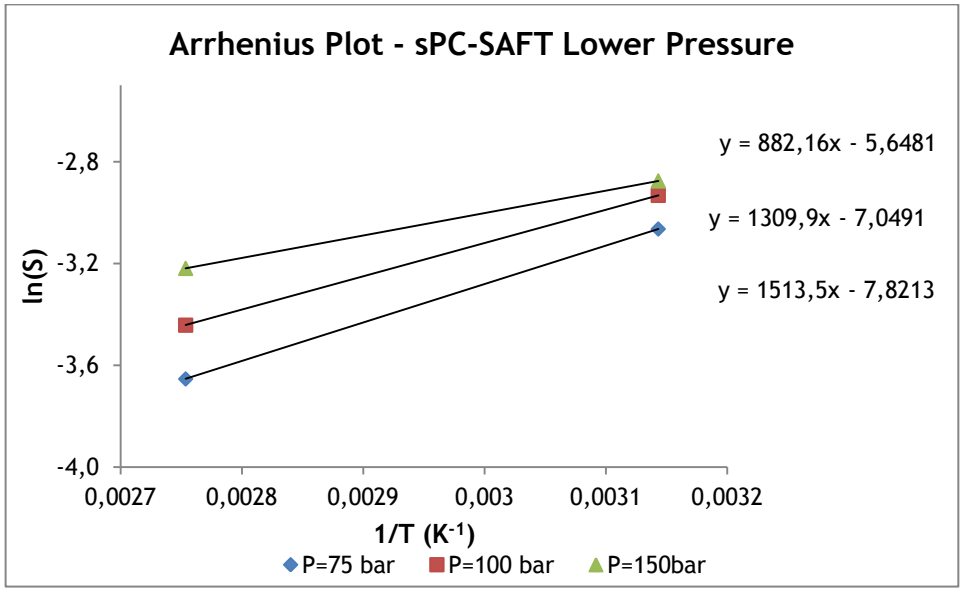

Figure A3.2 - Arrhenius plot for the modeled values of solubility (fitted to lower pressure data), for three pressures, in PVDF.

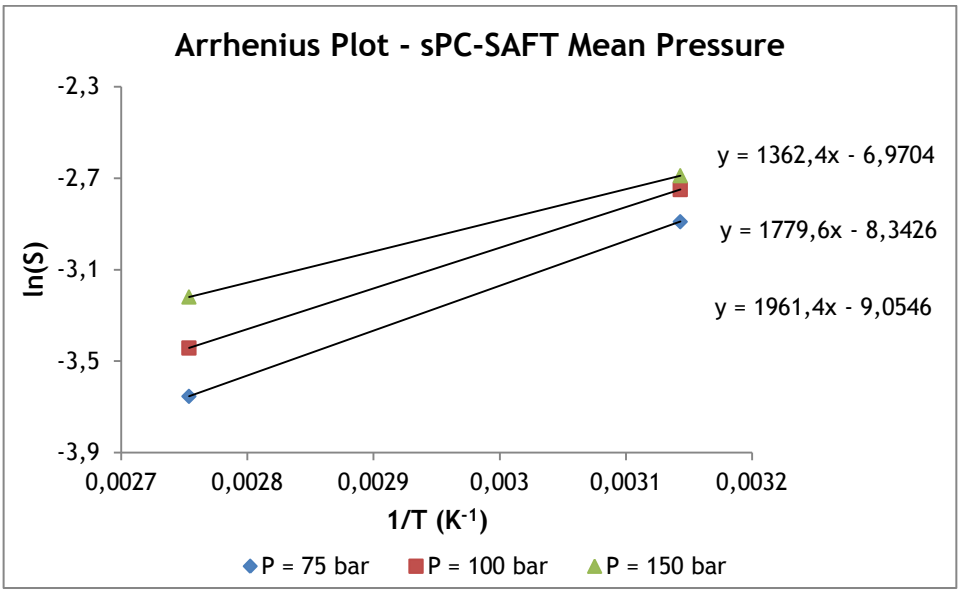

Figure A3.3 - Arrhenius plot for the modeled values of solubility (fitted to intermediate pressure data), for three pressures, in PVDF.

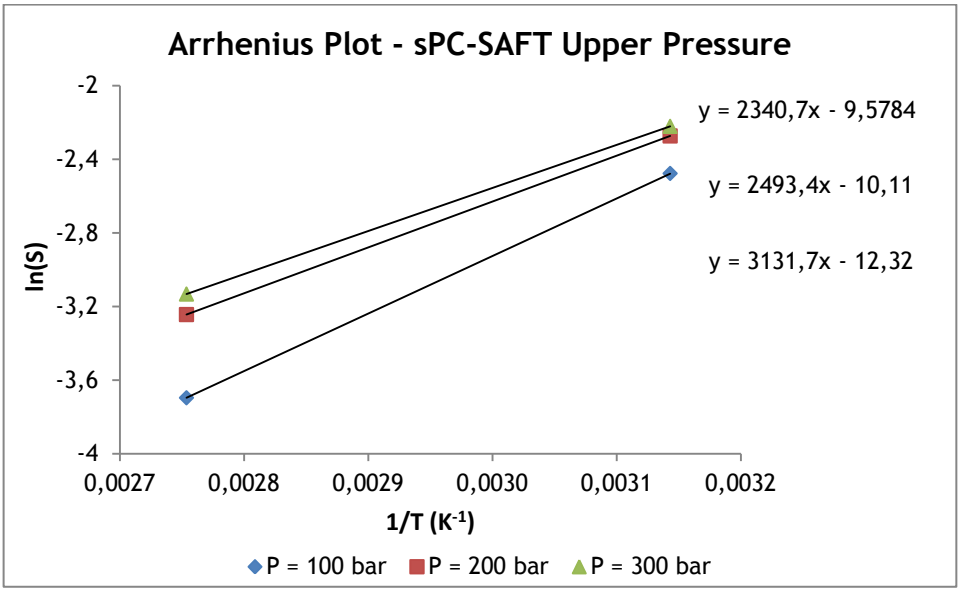

Figure A3.4 - Arrhenius plot for the modeled values of solubility (fitted to high pressure data), for three pressures, in PVDF.

- **XLPE**

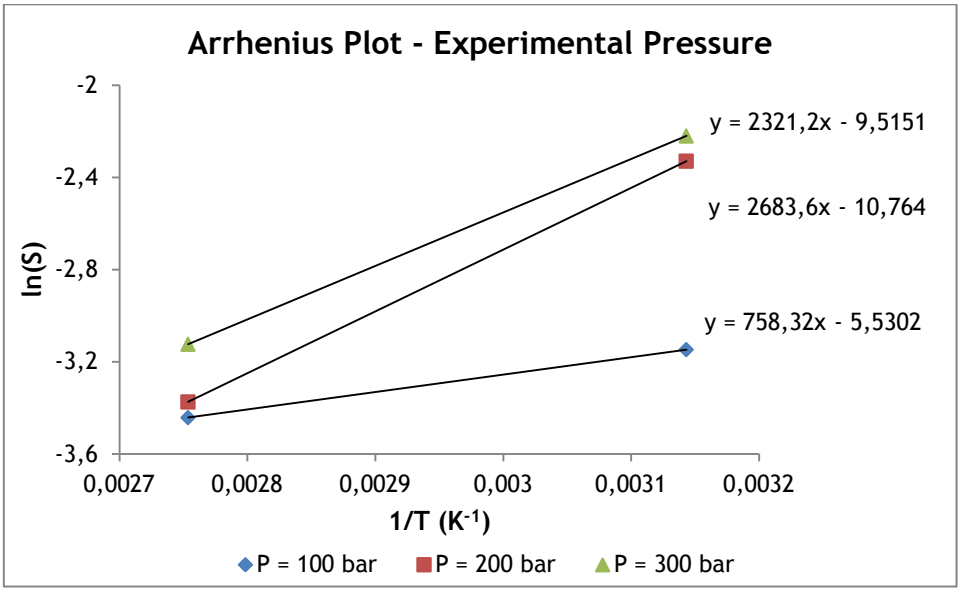

Figure A3.5 - Arrhenius plot for experimental solubility at three pressures, in XLPE.

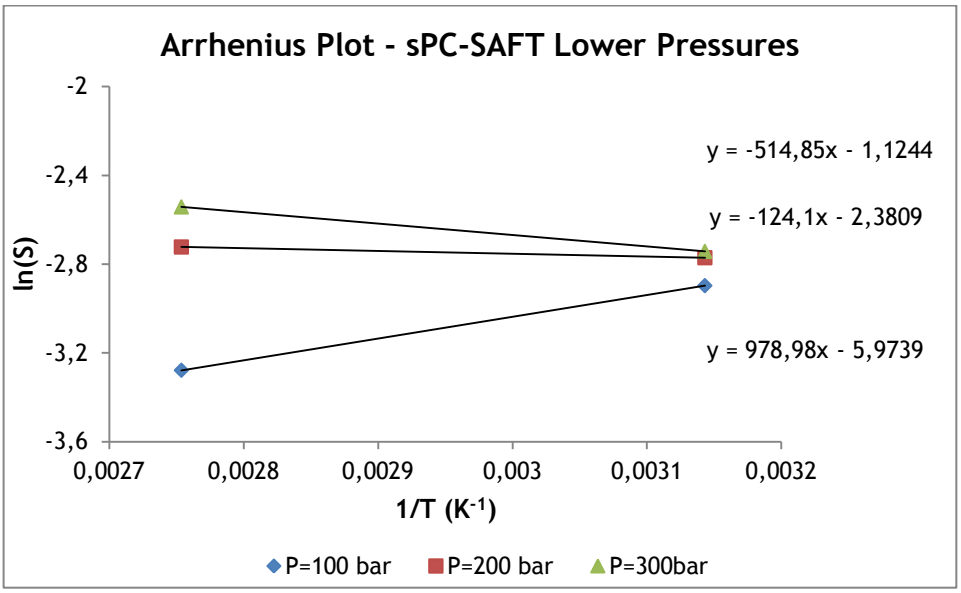

Figure A3.6 - Arrhenius plot for solubility modeled, respecting the lower pressure, at three pressures, in XLPE.

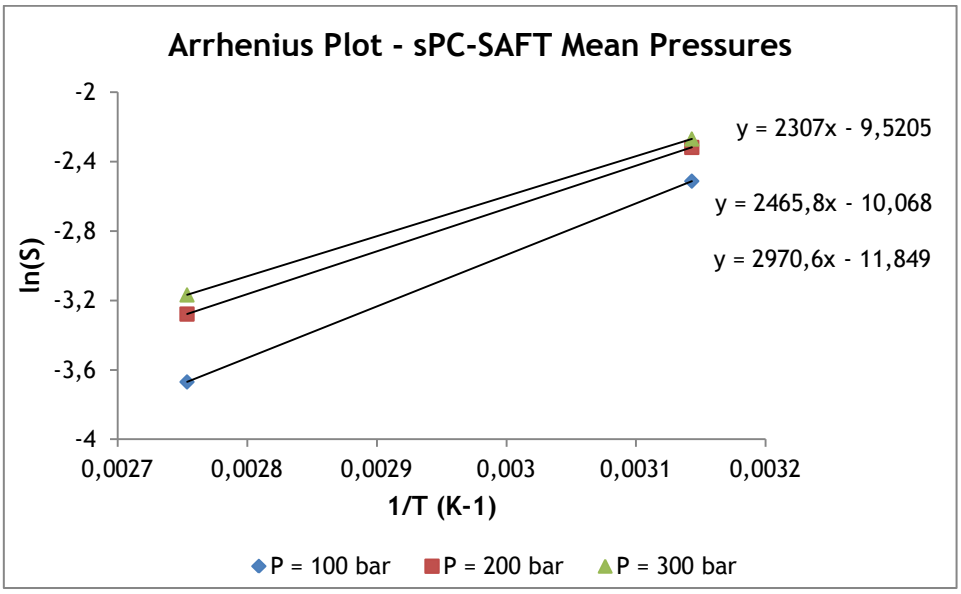

Figure A3.7 - Arrhenius plot for solubility modeled, respecting the intermediate pressure, at three pressures, in XLPE.

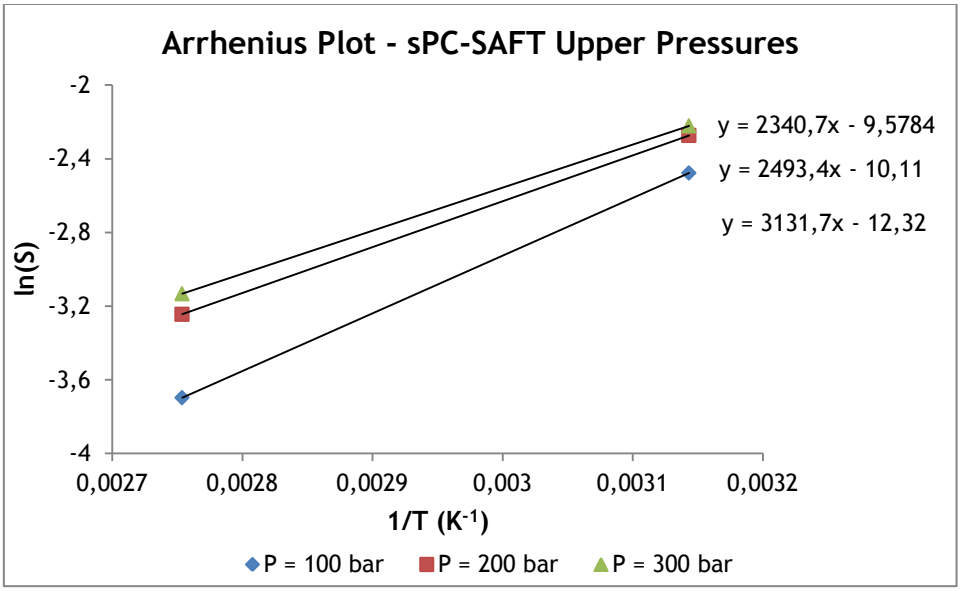

Figure A3.8 - Arrhenius plot for solubility modeled, respecting the upper pressure, at three pressures, in XLPE.

Appendix 4 - Influence of Temperature Graphs in Permeability

- **XLPE**

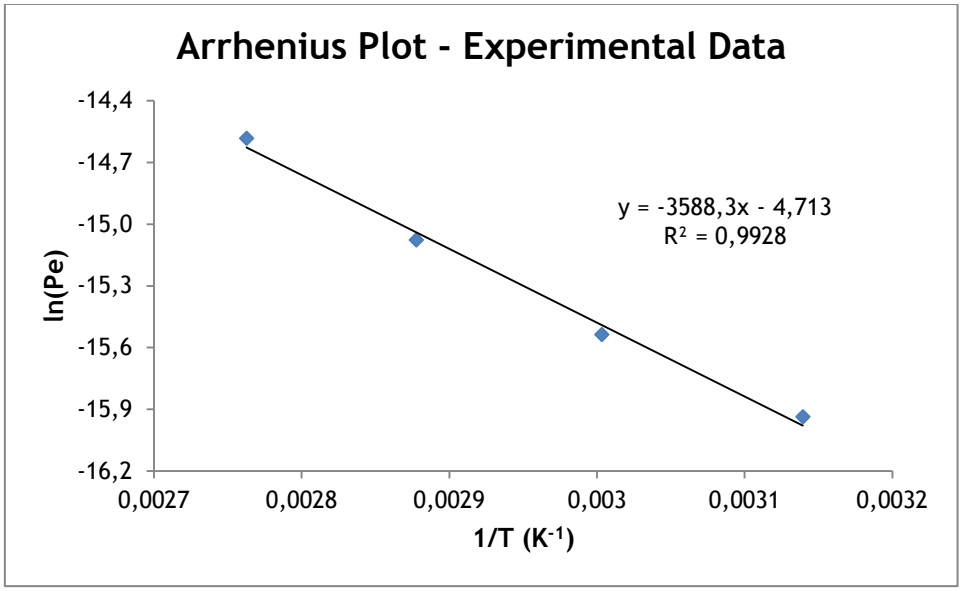

Figure A4.1 - Plot of 1/T vs ln(Pe) for the PVDF/CO_2 system at $P_{\text{High Pressure Chamber}}$ = 100 bar